THEORETICAL AND EXPERIMENTAL STUDY OF
MOLECULAR-BEAM MICROWAVE SPECTROSCOPY

MARTIN PETER

M. W. P. STRANDBERG

TECHNICAL REPORT 336

AUGUST 26, 1957

Loan Copy Only

RESEARCH LABORATORY OF ELECTRONICS
MASSACHUSETTS INSTITUTE OF TECHNOLOGY
CAMBRIDGE, MASSACHUSETTS

MASSACHUSETTS INSTITUTE OF TECHNOLOGY

RESEARCH LABORATORY OF ELECTRONICS

Technical Report 336   August 26, 1957

THEORETICAL AND EXPERIMENTAL STUDY OF MOLECULAR-BEAM
MICROWAVE SPECTROSCOPY

Martin Peter

M. W. P. Strandberg

Abstract

A variety of topics that bear directly upon the use of molecular-beam spectroscopic
methods for precise frequency determination with the use of alkali-halide molecules are
discussed. The rotational-energy spectrum, including resolvable hyperfine structure
arising from quadripole and magnetic interactions, is calculated. An analysis of inte-
grated line strength, or intensities, is presented. State selection is discussed in terms
of the appropriate high-field Stark effect, for which new calculations are given. State
selection with both axial and transverse-rod configurations is discussed, and trajectories
for sodium chloride with the use of a transverse-rod state selector are indicated. The
limitations of any state selector which arise from nonadiabatic losses are analyzed.
The design parameters of a microwave spectroscope, including signal-to-noise ratio
and ultimate precision, are related to its geometric configuration, and a description of
an apparatus that is adequate for high-resolution work is given. Related topics, such as
the concept of efficiency of frequency measurements and frequency pulling, are discussed
in generalized fashion. Conclusions that can be derived from this work, as to both pres-
ent limitations and necessary future development, are drawn.

Table of Contents

INTRODUCTION

Since the first successful experiment in molecular-beam microwave spectroscopy by Strandberg and Dreicer (1), this branch of spectroscopy has undergone rapid development. Soon afterward, Gordon, Zeiger, and Townes (2) developed the maser, in which the conditions of the beam experiment were adjusted for optimum signal-to-noise ratio by selecting the upper of the two ammonia inversion states and by matching the radiation out of the beam. This idea, which made the spectroscope operate as an oscillator or as an amplifier, has since been successfully applied in solid-state spectroscopy (3).

An increase in spectroscopic precision is desirable because a greater insight into the structure of matter will be gained thereby and because frequency standards of the highest precision and reproducibility can be derived from high-precision microwave spectroscopy. Although the research described in this report has not produced a usable instrument, it still seems worth while to describe the problems encountered in our attempt to reach that goal. We also present some results that were obtained in the course of this research — computation of the Stark effect of linear rotors, new schemes of phase stabilization, the development of hot-beam sources, the mode control of large cavities, and a discussion of the efficiency of frequency standards based on information theory — all of which should prove helpful in further research.

I. SPECTRUM OF SODIUM CHLORIDE

INTRODUCTION

One of the promising applications of the molecular-beam spectroscope is in the investigation of alkali halides. From this group of molecules, sodium chloride was selected because its spectrum is not very well known. Table I gives a survey of the present data on alkali halides. An understanding of this spectrum is necessary for the investigation. There are thirty 3/2-3/2 molecules listed in Table I. Hence we thought it worth while to reproduce some calculations of the quadripole and magnetic interactions that had been made for NaCl (Secs. II and III). In general, their spectra are well understood, but there has been little quantitative understanding of the electronic states, which would allow quantitative prediction of the microwave spectra. The intensive work on alkali hydrides by J. C. Slater and the Solid State and Molecular Theory group, M.I.T., gives promise of achieving such an understanding. It will be shown later that measurements of the alkali-halide spectra will provide several possibilities for comparison with calculated electronic wave functions.

1.1 HAMILTONIAN OF SODIUM CHLORIDE

The following interactions are of interest in the study of the spectra of alkali halides:

$$H = H_{nuc} + H_{el} + H_{vib} + H_{rot} + H_{rot\text{-}vib} + H_{rot\text{-}el}$$

$$+ H_{quadripole}$$

$$+ H_{magnetic}$$

$$+ H_{Stark}$$

$$+ H_{Zeeman}$$

$$+ H_{ext}$$

The terms listed on the first line (the nuclear, electronic, vibrational, rotational, rotational-vibrational, and rotational-electronic terms) will not be dealt with here. They are taken care of in the standard theory of diatomic molecules. It is well known that for precise measurements of equilibrium distances and nuclear mass, knowledge of the rotational-electronic interaction is required, and that this interaction can be obtained by measuring the molecular Zeeman effect (4). Zeeman-effect measurements are greatly facilitated by a system of high resolution. We can write $I = I_A + \Delta I$, where I_A is the moment of inertia calculated by using atomic masses at the nuclear positions. Hence

Table I. Rotational Constants and Oven Temperatures for Alkali Halides.

r (%)	I	A	Z		F	Cl	Cl	Br	Br	I
					100%	75.4%	24.6%	50.5%	49.5%	100%
					19	35	37	79	81	127
					9	17	17	35	35	53
					3/2, 1/2	3/2	3/2	3/2	3/2	5/2
7.5%	1/2	6	3	Li	985°	755°		727°	19,162.316†	690°; 15,381.986†
92.4%	3/2	7	3	Li	985°			16,651.186†	16,617.617†	13,286.785†
100%	3/2	23	11	Na	990°	845°; 6537.07†		785°; 4534.52†	4509.35†	770°; 3531.778†
93.1%	3/2	39	19	K	915°	812°; 3856.399*	3746.611*	790°; 2434.953*	2434.953*	750°; 1825.012†
6.9%	3/2	41	19	K		3767.421*				1756.903†‡
72.1%	5/2	85	37	Rb		717°; 2627.414*		1424.840†	1406.5944†‡	984.3166†
27.8%	3/2	87	37	Rb		2609.779*†		1409.0573†‡		970.7601†‡
100%	7/2	133	55	Cs	5527.34†	865°; 2161.208†	2068.761†‡	1081.3429†	1064.5853†‡	708.3579†

A tabulation according to abundance (r), spin (I), mass number (A), and atomic number (Z) for alkalies and halides of the resulting molecular constants, B_e (mc), and oven temperature (K) for $p = 1.4 \times 10^{-3}$ mm Hg of the resulting molecules.

*Molecular-beam measurement. [See N. F. Ramsey, Molecular Beams (Oxford University Press, London, 1956); R. Braunstein and J. W. Trischka, Phys. Rev. 98, 1092 (1955).]

†Microwave spectroscopy measurement. [See P. A. Tate and M. W. P. Strandberg, J. Chem. Phys. 22, 1380 (1953); A. Honig, C. H. Townes, M. L. Stitch, and M. Mandel, Phys. Rev. 96, 629 (1954).]

‡Y_{01} is quoted instead of B_e.

$$\Delta I = -\left[\sum_j N_S \, mJ \, r^2 - 2 \sum_n \frac{\hbar^2 |(0|L_x|n)|^2}{W_n - W_o}\right] \tag{1}$$

where $N_S = Z_S - N_{fS}$, Z_S is the atomic number, and N_{fS} is the number of electrons in the nearest filled shell. The sum

$$\sum \frac{\hbar^2 |(0|L_x|n)|^2}{W_n - W_o}$$

is a measure of the electronic orbital angular momentum induced in the ground state; it was evaluated only for the electrons in the unfilled shell. Since W_n is not known for NaCl, as a crude approximation we neglect this sum and take

$$N_{Na} = +1, \quad N_{Cl} = -1, \quad J_{Na} = 1.42 \text{ A}, \quad J_{Cl} = 0.93 \text{ A}$$

$$\frac{\Delta I}{I} = -8.2 \times 10^{-6}, \quad g_J = -\frac{m_P}{m_e} \qquad \frac{\Delta I}{I_A} = +0.015$$

Johnson and Strandberg's comparison of calculations with measurements (5) indicates that such an estimate is uncertain, even with respect to sign, but at least it will give the order of magnitude. As long as $|L|$ is a constant of the motion [cf. Tinkham (6)], the evaluation of $|(0|L_x|n)|^2$ is simple, and the measurement of the Zeeman effect might be used to locate the unobserved lowest electronic energy levels. We expected to observe the Zeeman splitting with a field of 100 gauss, since the splitting is 20 cps per gauss, and the half-halfwidth of the line was to be 500 cps.

Another perturbation that is of second order in the electronic angular momentum is the "cosine interaction." The off-diagonal elements of L are weighted differently, so that the measurement of g_J, C_{I_1}, and C_{I_2} would provide us with three independent equations containing matrix elements of L. A crude estimate of the order of magnitude of C_I is obtained from $C_I \approx 2g_J g_I \mu_n^2 \frac{1}{r^3}$, or $C_I \approx 2.8$ kc (with $r = 0.4$ A). $H_{quadripole}$ will be treated in section 1.2, $H_{magnetic}$ in section 1.3, H_{ext} in section 1.4, and H_{Stark} in Section II.

1.2 DOUBLE QUADRIPOLE INTERACTION

The diatomic molecule, in which both atoms show a quadripole moment, has been treated by Bardeen and Townes (7). For this case, we have $\nu = \nu_o + \Delta\nu_1 + \Delta\nu_2$. Here

$$\Delta\nu_1 (F_1) = +\, eqQ_L \, \frac{I_1(I_1 + 1) \, J(J + 1) - \frac{3}{4} C(C + 1)}{2I_1(2I_1 - 1)(2J - 1)(2J + 3)} \tag{2}$$

in which C is the Casimir function: $C = F_1(F_1 + 1) - I(I+1) - J(J+1)$.

$$\Delta\nu_2 = \sum c^2 (F_1 F_2) \Delta'\nu_2(F_2)$$

with $\Delta'\nu_2$ calculated as $\Delta\nu_1$, but with I_2, F_2, eqQ_2 replacing I_1, F_1, eqQ_1. The transformation coefficients $c^2(F_1 F_2)$ are given by

$$c^2(F_1, F_2) = (2F_1 + 1)(2F_2 + 1) W^2(F_1, 3/2, 3/2, F_2; F, J)$$

in which the W functions are the Racah coefficients tabulated by Simon, Vander Sluis, and Biedenharn(8). Results of the calculations for the 3/2-3/2 molecules are given in Fig.1.

1.3 MAGNETIC INTERACTION

Magnetic interactions arise from the interaction of the two nuclei with each other, and from the interaction of each nucleus with the rotational-magnetic moment of the molecule (7).

We write, classically,

$$W = \frac{(\vec{\mu}_1 \cdot \vec{\mu}_2)}{r^3} - 3 \frac{(\vec{\mu}_1 \cdot \vec{r})(\vec{\mu}_2 \cdot \vec{r})}{r^5} \tag{3}$$

which can be transformed into

$$H = \frac{\mu_n^2 g_1 g_2}{r^3} [(\vec{I}_1 \cdot \vec{I}_2) - 3(\vec{I}_1 \cdot \vec{k})(\vec{I}_2 \cdot \vec{k})] \tag{4}$$

where k is the unit vector in the molecular axis. The matrices for $(\vec{I}_1 \cdot \vec{I}_2)$ and $(\vec{I}_2 \cdot \vec{k})$ are given by adapting the results of Frosch and Foley (9). They do not give the matrix $(\vec{I}_1 \cdot \vec{k})$ for $I_1 = 3/2, I_2 = 3/2$. It can be found either by transforming $(\vec{I}_2 \cdot \vec{k})$ in the $J\ I_1\ F_1\ I_2\ F\ M_F$ representation into the $J\ I_2\ F_3\ I_1\ F\ M_F$ representation, by means of Racah coefficients, or directly (10). The elements have the following values:

$F_1 = F_1'$	J	J'	$(J\ I_1\ F_1\ I_2\ F\ M_F \vert I_1 \cdot k \vert J'\ I_1\ F_1'\ I_2\ F\ M_F)$
$J - \frac{3}{2}$	J	J - 1	$\frac{\sqrt{3}}{2}\sqrt{\frac{2J-3}{2J-1}}$
$J - \frac{1}{2}$	J	J - 1	$2\sqrt{\frac{(J-1)(J+1)}{(2J-1)(2J+1)}}$
$J - \frac{1}{2}$	J + 1	J	$\frac{\sqrt{3}}{2}\sqrt{\frac{2J-1}{2J+1}}$
$J + \frac{1}{2}$	J	J - 1	$\frac{\sqrt{3}}{2}\sqrt{\frac{2J+3}{2J+1}}$
$J + \frac{1}{2}$	J + 1	J	$2\sqrt{\frac{J(J+2)}{(2J+1)(2J+3)}}$
$J + \frac{3}{2}$	J + 1	J	$\frac{\sqrt{3}}{2}\sqrt{\frac{2J+5}{2J+3}}$

F_1

J=1   F

0.2500 x (eqQ$_1$)

-0.0046 (-eqQ$_2$)   2

$\frac{1}{2}$

-0.0002 (-eqQ$_2$)   1

$\frac{5}{2}$ 0.0500 x (-eqQ$_1$)

-0.110 (-eqQ$_2$)   3

-0.020 (-eqQ$_2$)   2

0.0500 (-eqQ$_2$)   4

0.140 (-eqQ$_2$)   1

$\frac{3}{2}$ -0.2000 x (-eqQ)

-0.200 (-eqQ$_2$)   0

-0.108 (-eqQ$_2$)   1

-0.40 (-eqQ$_2$)   3

0.118 (-eqQ$_2$)   2

J=2

$\frac{1}{2}$ 0.250 x (-eqQ$_1$)

0.000 (-eqQ$_2$)   2

0.003 (-eqQ$_2$)   1

$\frac{7}{2}$ 0.0714 x (-eqQ$_1$)

-0.132 (-eqQ$_2$)   4

-0.051 (-eqQ$_2$)   3

0.000 (-eqQ$_2$)   5

0.153 (-eqQ$_2$)   2

$\frac{3}{2}$ 0.000 x (-eqQ$_1$)

0.000 (-eqQ$_2$)   0

0.000 (-eqQ$_2$)   1

0.000 (-eqQ$_2$)   3

0.030 (-eqQ$_2$)   2

$\frac{5}{2}$ -0.1785 x (-eqQ$_1$)

-0.060 (-eqQ$_2$)   3

-0.012 (-eqQ$_2$)   2
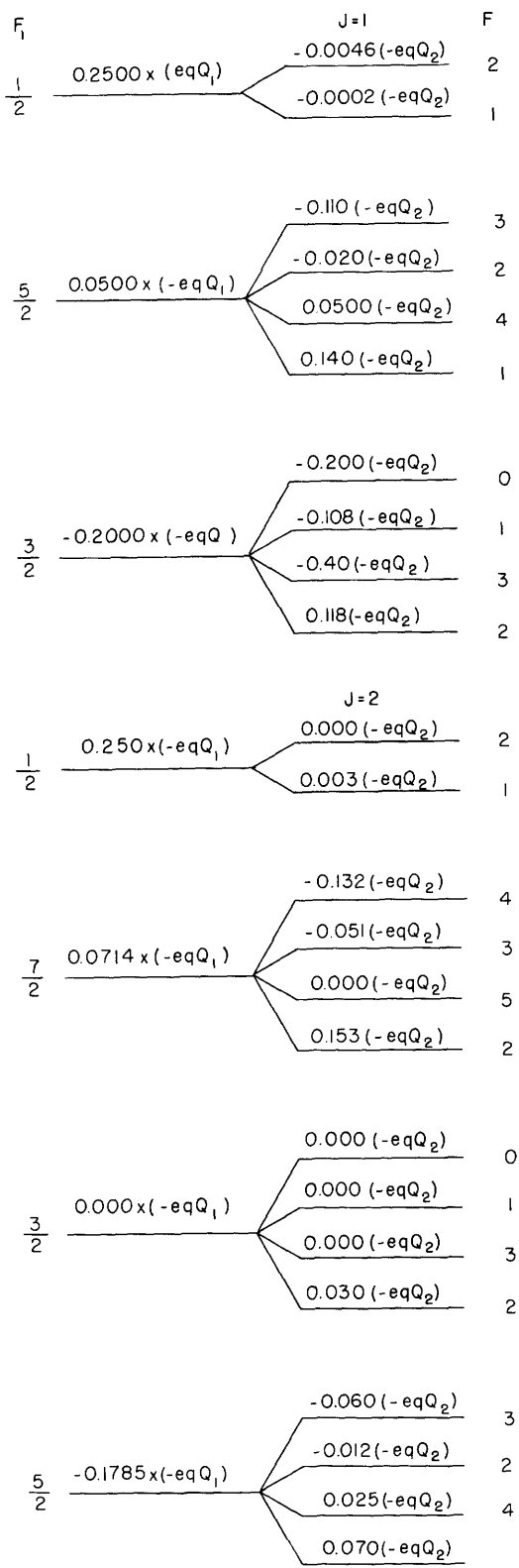
0.025 (-eqQ$_2$)   4

0.070 (-eqQ$_2$)

Fig. 1. Double quadripole coupling for J=1, J=2 transition in 3/2-3/2 molecule, with eqQ$_1$ ≫ eqQ$_2$.

6

The diagonal elements of $(\vec{I}_1 \cdot \vec{J}_1)$, $(\vec{I}_2 \cdot \vec{J}_1)$, $(\vec{I} \cdot \vec{I}_2)$ can be found with the aid of a vector model, to which we add the rotational interactions of the nuclei. Hence the magnetic interaction takes the following form:

$$W_{(J\, I_1\, F_1\, I_2\, F\, M_F)} = \frac{1}{2}\, C_{I_1} \left\{ F_1(F_1+1) - J(J+1) - I_1(I_1+1) \right\}$$

$$+ C_{I_2} \frac{\left\{ F(F+1) - F_1(F_1+1) - I_2(I_2+1) \right\} \left\{ F_1(F_1+1) + J(J+1) - I_1(I_1+1) \right\}}{4F_1(F_1+1)}$$

$$+ \frac{\mu_n^2\, g_{I_1}\, g_{I_2} \left\{ F(F+1) - F_1(F_1+1) - I_2(I_2+1) \right\}}{2r^3} \begin{cases} 6\dfrac{J+1}{(2J-1)} & F_1 = J - \dfrac{3}{2} \\[2ex] \dfrac{4J^2 + 26J - 32}{(2J+1)(2J-1)^2} & F_1 = J - \dfrac{1}{2} \\[2ex] \dfrac{-4J^2 + 18J + 54}{(2J+1)(2J+3)^2} & F_1 = J + \dfrac{1}{2} \\[2ex] \dfrac{-6J}{(2J+3)^2} & F_1 = J + \dfrac{3}{2} \end{cases} \qquad (5)$$

1.4 SIGNAL INTENSITIES

In order to calculate the observable signal, we shall have to know the partition sum, Z, and the transition matrix elements. Of the total number of molecules, n_t, only a fraction participates in the actual transition. For NaCl, the low-lying energy states are populated by a fraction

$$f = \frac{1}{Z_{rot}} \frac{1}{Z_{vib}} \frac{1}{Z_{nuc}}$$

$$Z_{rot} \approx \frac{kT}{hB} = 2540$$

with $T = 848°$ K, $B = 6536.86$, and $\nu_{vib} = 1.15 \times 10^{13}$. We obtain

$$Z_{vib} = \frac{1}{1 - \exp(-h\nu_{vib}/kT)} = 2.9$$

$$Z_{nuc} = (2I_1 + 1)(2I_2 + 1) = 16$$

which yields

$$f = \frac{1}{119,000}$$

It can be seen from Fig. 1 that, in general, several quantum states belong to the same energy level. In the first place, there is degeneracy for all M_F-states that belong

7

to the same F-level. There may also be accidental degeneracy between different F-levels. Or, F-levels may not be degenerate but the transition frequencies between them may accidentally coincide. By coincidence we mean that the levels are closer than 1 kc, since 1 kc is the linewidth that we expect to observe. Let us write $\mu\gamma_{ij}$ for the dipole moment that is effective for the transition from state i to state j; here j stands for a set of quantum numbers J, F_1, F, M_F. Since the γ_{ij} are different for different states, it is apparent that for a number of degenerate states the transition condition (see sec. 3.1) can only be fulfilled for one state. The other states will have made incomplete transitions in the spectroscope cavity. In the following discussion we do find the conditions for an optimum signal, but carry the calculation through for a certain power level in the signal cavity, P_o. Thereafter, the true optimum signal can be found experimentally.

We take $\gamma_o = \max(\gamma_{ij})$ and adjust the power so that the state with the strongest dipole moment is totally flipped. Then the total number of transitions, including the partially flipped states, becomes

$$d = \Sigma \sin^2\left(\frac{\gamma_{ij}}{\gamma_o}\frac{\pi}{2}\right) \qquad (6)$$

The sum is taken over all transitions of the same frequency. Our signal then becomes proportional to $I = d^2\gamma_o^2$, as will be shown in Section III. For numerical evaluation, an approximation has been introduced:

$$\sin\left(\frac{\gamma_{ij}}{\gamma_o}\frac{\pi}{2}\right) \approx \frac{\gamma_{ij}}{\gamma_o}$$

Although it is not difficult to calculate the matrix elements μ_{ij}, the aforementioned simplification permits the use of values given in published works. Thus we find that

$$I = \left(\frac{\displaystyle\sum_{M_F;M'_{F'}}\gamma_{ij}^2}{\gamma_o^2}\right)^2 \gamma_o^2 \qquad (7)$$

The summation is over the degenerate states M_F, $M'_{F'}$, that belong to our transition. Because of the marked differences in the level shift for the subsequent quantum numbers J, F_1, F, we obtain

$$\sum_{M_F;M'_{F'}}\gamma_{ij}^2 = \left(I_{F,F';F_1,F'_1}\right)\left(I_{F_1,F'_1;J,J'}\right)(I_{J,J'}) \qquad (8)$$

8

with $I_{J, J+1} = \frac{J+1}{3}(2I_1+1)(2I_2+1)$. For our case, $I_{F_1, F_1';J, J'}$ and $I_{F, F';F_1, F_1'}$ are given in reference 11. Furthermore,

$$\gamma_0^2 = \sum_{M_F; M'_{F'}} \gamma_{ij}^2 \, K(F, F')$$

where

$$\left. \begin{array}{l} K = \dfrac{3(F+1)}{(2F+1)(2F+3)} \quad \text{for } F' - F = +1 \\[2ex] K = \dfrac{3F}{(2F+1)(F+1)} \quad \text{for } F' - F = 0 \\[2ex] K = \dfrac{3F}{(2F+1)(2F-1)} \quad \text{for } F' - F = -1 \end{array} \right\} \tag{9}$$

Whence we obtain

$$I = \left(\frac{1}{K_{F, F'}}\right)(I_{J;J'})\left(I_{F_1, F_1';J, J'}\right)\left(I_{F, F'; F_1, F_1'}\right) \tag{10}$$

as a measure of the intensity with which the lines appear. I is given with the transitions in Fig. 2.

We find that

$$I_{max} = 9.2 \text{ for the transition}$$

$$\left. \begin{array}{l} J = 1 \\ F = 5/2 \\ F = 4 \end{array} \right\} \longleftrightarrow \left\{ \begin{array}{l} J' = 2 \\ F_1' = 7/2 \\ F' = 5. \end{array} \right.$$

(For future reference, we define $I = d \cdot \mu_{ij}$; where d is defined by Eq. 6 and μ_{ij} is the effective dipole moment.)

1.5 SPECTRUM IN THE BEAM APPARATUS

The spectrum shown in Fig. 2 has been evaluated by using the value $eqQ_{Na} = -5.4$ mc, given by Logan, Cote, and Kusch (12); eqQ_{Cl} was not measured. It can be estimated by extrapolating from known quadripole values. We find a regular progression in eqQ if we write the molecules in the order of increasing electronegativity, as shown by Dailey and Townes (13):

KI : KBr : KCl = -60 : 10.2 : -0.03

LI : LiBr = -198.5 : 37.2

NaI : NaBr : NaCl = -259 : 58 : x

9

Fig. 2. Energy-level diagram for J=1, J=2 transition in NaCl.
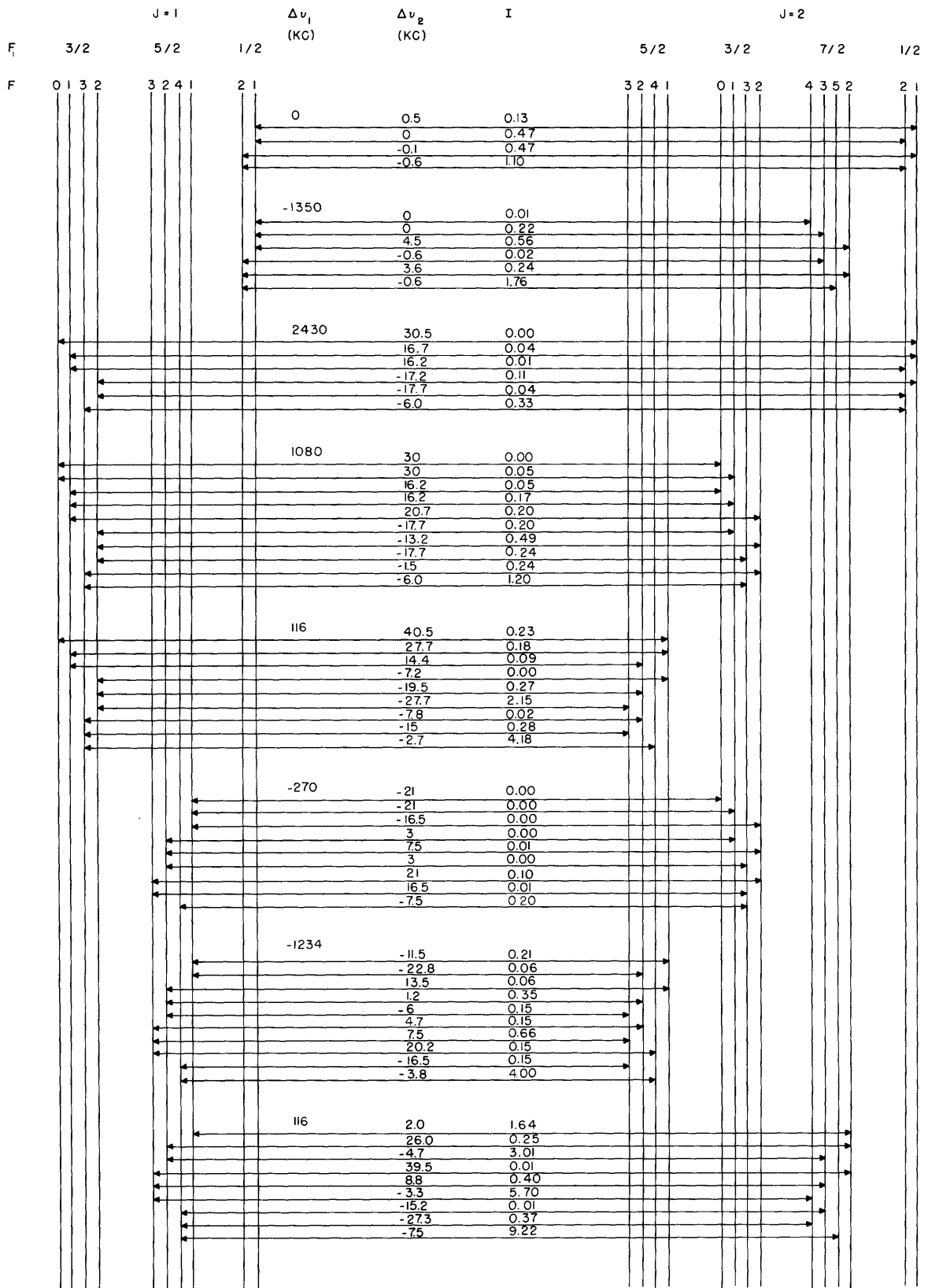
eqQ$_{Na}$ = -5.4MC , eqQ$_{Cl}$ = -150KC , NO MAGNETIC COUPLING

10

The value and sign of KCl are given by Lee, Fabricand, Carlson, and Rabi (14); values for the others are taken from Honig, Townes, Stitch, and Mandel (15). It is merely stated that eqQ_{Cl} is negative, with an absolute value smaller than 0.04. Thus our value, $eqQ_{Cl} = -150$ kc, is only an estimate that is compatible with present knowledge. The spectrum for these values was plotted in order to visualize the spectrum that would be expected in the beam spectrometer. Estimates of the magnetic interactions were found to be small enough so that they could be neglected in this prediction. These interesting interactions can, probably, only be detected by using a molecular beam in a large interaction-cavity spectroscope, as described here, or by a conventional molecular-beam apparatus with stimulating radiation of the highest stability.

II. HIGH-FIELD STARK EFFECT AND ELECTROSTATIC STATE SELECTION

INTRODUCTION

The problem of state selection in molecular-beam microwave spectroscopy has been successfully solved by Gordon and Townes, who used a design of Bennewitz, Paul, and Schlier (16). However, a direct application of this work is not compatible with our goal of obtaining high inherent precision, since the maser focuser transforms the initially collimated parallel beam into a divergent beam. Therefore we set out to make a focuser which, like the cylindrical lens, will deflect the particles only in one plane, so that in the direction of the 17 nodes of our cavity, the molecules would not have any velocity components. A knowledge of high-field Stark effect is of importance in this connection, and therefore the solution of this problem will be given below, and the efficiency of our Stark selector can then be evaluated.

2.1 HIGH-FIELD STARK EFFECT

The influence of a static electric field on a rotor was calculated with the use of ordinary stationary perturbation theory. The zero-order functions are the functions of the free rotor. The perturbation calculation gives the energy levels in terms of a series in λ, which converges for small values of $\lambda(\lambda < J)$. The following symbols are used:

$$\lambda = \frac{\mu F}{hB}$$

$$W = \frac{E}{hB}$$

J, K, M

$m = |M|$

$\xi = (a)^{1/2} r$

$a = (\lambda/2)^{1/2}$

$$\beta_t = \frac{W^{(t)} + \lambda}{a}, \quad \beta = \frac{W + \lambda}{a}$$

μ = molecular dipole moment

F = static field

$B = h/8\pi^2 I$ = reduced moment of inertia

reduced energy

symmetric-top quantum numbers

For higher values of λ, the procedure becomes inadequate, and the equations of motion might have to be solved exactly. In the cases of the symmetric and linear rotors, a continued-fraction method for the evaluation of $W_{(J, M, K, \lambda)}$ is available (17, 18). Barriol (19) mentions an asymptotic formula for the two-dimensional rigid rotor, for the case in which $\lambda > W$.

12

We want to find a power series in $\lambda^{-1/2}$ for W that converges when the electric energy is larger than the rotational energy. This series can also be obtained from stationary perturbation theory, but the zero-order function will then correspond to very large fields, in which the rotor is eventually bound to an axis (direction of the electric field vector). The problem is then of the kind encountered in the treatment of vibrating rotors. Here, the rigid linear rotor is treated. It differs slightly from the general case because of the absence of a moment of inertia along the axis of symmetry. Energy levels for the linear rotor have been calculated by using Lamb's expression, which permits an evaluation of the convergence of our approximation.

a. Harmonic Oscillator Approximation for the Rigid Linear Rotor

The wave equation for the rigid linear rotor in the presence of an electric field is

$$0 = \left[\frac{1}{\sin\theta}\frac{\partial}{\partial\theta}\sin\theta\frac{\partial}{\partial\theta} + \frac{1}{\sin^2\theta}\frac{\partial^2}{\partial\phi^2} + W + \lambda\cos\theta \right]\psi \qquad (11)$$

The continued fraction for W is

$$W = m(m+1) - \lambda^2 \left. \frac{(m+1)^2 - m^2}{(2m+1)(2m+3)} \right/ (m+1)(m+2)$$

$$-W - \lambda^2 \left. \frac{(m+2)^2 - m^2}{(2m+3)(2m+5)} \right/ (m+2) \ldots \qquad (12)$$

The following coordinate transformation gives a more convenient form to Eq. 11:

$$r = 2\tan(\theta/2)$$

$$\phi = \phi$$

Equation 11 then reads

$$\left(1 + \frac{r^2}{4}\right)^2\left(\frac{\partial^2}{\partial r^2} + \frac{1}{r}\frac{\partial}{\partial r} + \frac{1}{r^2}\frac{\partial^2}{\partial\phi^2}\right)F(r,\phi) + \left[W + \lambda\frac{4 - r^2}{4 + r^2}\right]F(r,\phi) = 0 \qquad (13)$$

Let $F(r,\phi) = \Phi(\phi)U_{(n,m)}(\xi)$, where $\Phi(\phi) = \dfrac{1}{(2\pi)^{1/2}}e^{im\phi}$; and thus we find that

$$\left\{\left(1 + \frac{\xi^2}{4a}\right)^2\left(\frac{d^2}{d\xi^2} + \frac{1}{\xi}\frac{d}{d\xi} - \frac{m^2}{\xi^2}\right) + \beta - \xi^2 + \frac{\xi^4}{4a} - \frac{\xi^6}{16a^2}\right.$$

$$\left. + \frac{\xi^8}{64a^3} - \frac{\xi^{10}}{256a^4}\ldots\right\}U_{(n,m)}(\xi) = 0 \qquad (14)$$

For $a \to \infty$, this equation is encountered in the treatment of the two-dimensional harmonic

oscillator (20), with the solutions

$$U_{(n,m)} = N_{(n,m)} \exp(-\xi^2/2)\, \xi^m$$

$$\times \left[1 + \sum_{\nu=2,4,\ldots}^{n} (-1)^{\nu/2} \right.$$

$$\left. \times \frac{n(n-2)\ldots(n-\nu+2)}{2\times 4\times\ldots\times\nu(m+1)(m+2)\ldots(m+\nu/2)}\, \xi^\nu \right]$$

$$\beta_0 = 2(m+n+1)$$

The energy levels can now be expanded in a:

$$W_{(n,m)} = W^{(o)}_{(n,m)} + W^{(1)}_{(n,m)}\, a^o + W^{(2)}_{(n,m)}\, a^{-1} + \ldots$$

and so can the equation of motion:

$$\left(H_0 + a^{-1} H_1 + a^{-2} H_2 + \ldots \right) U_{nm} = \left(\beta_0 + a^{-1}\beta_1 + \ldots \right) U_{nm}$$

Herein

$$H_0 = \left(-\frac{d^2}{d\xi^2} - \frac{1}{\xi}\frac{d}{d\xi} + \frac{M^2}{\xi^2} \right) + \xi^2$$

$$H_1 = \frac{1}{2}\xi^2 \cdot \beta_0 - \frac{3}{4}\xi^4$$

$$H_2 = \frac{\xi^4}{16} \cdot \beta_0$$

$$\sum_{t=3}^{t=\infty} H_t = \frac{-\xi^8}{64}\, \frac{1}{1+(\xi^2/4a)}$$

In writing the higher-order terms H_1, H_2, and so forth, use has been made of the zero-order equation in order to substitute $\beta_0 - \xi^2$ for the differential operator

$$\left(-\frac{d^2}{d\xi^2} - \frac{1}{\xi}\frac{d}{d\xi} + \frac{M^2}{\xi^2} \right)$$

The matrices for ξ^2 and ξ^4 are easily calculated by writing $\xi^2 U_{nm}$ as a linear combination of $U_{n'm}$. [They have been tabulated by Shaffer (21).] Then we find

14

$$(m, n \,|\, H_1 \,|\, m, n - 2) = - \frac{3}{16} \left[(n-2)\, n(2m + n - 2)\, (2m + n) \right]^{1/2}$$

$$(m, n \,|\, H_1 \,|\, m, n - 1) = \frac{1}{4}\, (m + n + 2) \left[n(2m + n) \right]^{1/2}$$

$$(m, n \,|\, H_1 \,|\, m, n) = \frac{1}{8} \left[2m^2 - 2mn - n^2 - 2m - 2n - 4 \right]$$

$$(m, n \,|\, H_1 \,|\, m, n + 1) = \frac{1}{4}\, (m+n) \left[(n+2)(2m + n + 2) \right]^{1/2}$$

$$(m, n \,|\, H_1 \,|\, m, n + 2) = - \frac{3}{16} \left[(n+2)(n+4)(2m + n + 2)\, (2m + n + 4) \right]^{1/2}$$

$$(m, n \,|\, H_2 \,|\, m, n) = \frac{1}{16}\, (2m^2 + 6mn + 3n^2 + 6m + 6n + 4)(m + n + 1)$$

The matrices H_1 and H_2 are non-Hermitian. This is so because U_{nm} is normalized — not in the θ, ϕ space, but in the tangential r, ϕ plane. Nevertheless, it is easily verified that the $W_{n, m}^{(t)}$ are found as in the usual perturbation calculations; for example,

$$W_{(n, m)}^{(2)} = {\sum}' \frac{(mn \,|\, H_1 \,|\, mn')(mn' \,|\, H_1 \,|\, mn)}{W_{(n, m)}^{(o)} - W_{(n', m)}^{(o)}} + (mn \,|\, H_2 \,|\, mn)$$

Note that m is a good quantum number for all values of λ, because of the axial symmetry of the configuration. It is therefore possible to connect the levels at $\lambda = 0$ with the levels at $\lambda = \infty$, and we find that $n = 2(J-m)$. Now, n and m are eliminated and W is given in the more familiar quantum numbers J and M:

$$W_{(J, M)} = - \lambda^1 + \sqrt{2}[2J - |M| + 1]\, \lambda^{1/2}$$

$$+ \frac{1}{4} \left[M^2 + 2|M|\, J - 2J^2 + |M| - 2J - 2 \right] \lambda^0$$

$$+ \frac{\sqrt{2}}{64} \left[-4|M^3| + 6M^2 J + 6|M|\, J^2 - 4J^3 + 3M^2 \right.$$

$$\left. + 6|M|\, J - 6J^2 + 3|M| - 6J - 2 \right] \lambda^{-1/2} + \dots$$

In Table II, $W_{(J, M)}$ has been tabulated to $J = 4$ and $\lambda = 100$. The calculations were

Table II.

λ	W 0,0	W 1,0	W 1,1	W 2,0	W 2,1	W 2,2	W 3,0	W 3,1	W 3,2	W 3,3	W 4,0	W 4,1	W 4,2	W 4,3	W 4,4
0	0.00	2.00	2.00	6.00	6.00	6.00	12.00	12.00	12.00	12.00	20.00	20.00	20.00	20.00	20.00
1	−0.16	2.09	1.95	6.02	6.01	5.97	12.01	12.01	12.00	11.99	20.01	20.01	20.00	20.00	19.99
2	−0.56	2.29	1.81	6.10	6.04	5.91	12.04	12.03	12.00	11.94	20.03	20.02	20.01	19.99	19.96
3	−1.09	2.48	1.57	6.28	6.08	5.79	12.10	12.07	12.00	11.88	20.06	20.05	20.02	19.98	19.92
4	−1.70	2.60	1.27	6.41	6.12	5.63	12.18	12.13	11.99	11.78	20.10	20.09	20.04	19.96	19.86
5	−2.37	2.64	0.90	6.65	6.15	5.43	12.29	12.20	11.98	11.66	20.16	20.14	20.06	19.94	19.77
6	−3.06	2.59	0.49	6.91	6.15	5.19	12.42	12.29	11.96	11.51	20.24	20.20	20.09	19.91	19.68
7	−3.78	2.46	0.03	7.18	6.13	4.92	12.58	12.38	11.93	11.34	20.32	20.27	20.12	19.88	19.56
8	−4.52	2.26	−0.46	7.44	6.08	4.61	12.77	12.48	11.89	11.14	20.42	20.35	20.15	19.83	19.43
9	−5.28	2.02	−0.98	7.68	5.99	4.27	12.99	12.58	11.84	10.92	20.54	20.44	20.18	19.78	19.28
10	−6.05	1.72	−1.52	7.88	5.87	3.91	13.23	12.68	11.77	10.69	20.67	20.55	20.21	19.72	19.11
11	−6.83	1.39	−2.09	8.03	5.72	3.53	13.51	12.78	11.68	10.42	20.82	20.66	20.25	19.65	18.93
12	−7.62	1.03	−2.68	8.14	5.54	3.12	13.81	12.87	11.57	10.15	20.98	20.78	20.28	19.57	18.74
13	−8.42	0.64	−3.28	8.20	5.33	2.69	14.12	12.94	11.45	9.85	21.16	20.91	20.30	19.49	18.53
14	−9.22	0.23	−3.89	8.22	5.09	2.24	14.43	13.01	11.31	9.53	21.37	21.04	20.33	19.39	18.30
15	−10.04	−0.21	−4.52	8.20	4.83	1.78	14.74	13.05	11.16	9.20	21.59	21.18	20.35	19.28	18.06
16	−10.86	−0.66	−5.17	8.14	4.54	1.30	15.03	13.08	10.98	8.85	21.83	21.33	20.36	19.16	17.81
17	−11.68	−1.13	−5.82	8.05	4.24	0.81	15.32	13.09	10.79	8.49	22.09	21.47	20.37	19.03	17.55
18	−12.51	−1.62	−6.48	7.92	3.91	0.30	15.57	13.08	10.59	8.12	22.37	21.62	20.36	18.88	17.27
19	−13.35	−2.13	−7.15	7.77	3.57	−0.22	15.81	13.05	10.36	7.73	22.66	21.76	20.35	18.73	16.98
20	−14.19	−2.64	−7.83	7.60	3.21	−0.75	16.01	13.00	10.13	7.32	22.98	21.90	20.34	18.56	16.86
25	−18.44	−5.39	−11.34	6.42	1.20	−3.55	16.60	12.48	8.72	5.15	24.64	22.50	20.08	17.57	15.01
30	−22.76	−8.35	−15.00	4.85	−1.09	−6.56	16.55	11.56	7.02	2.74	26.15	22.83	19.56	16.32	13.11
35	−27.14	−11.48	−18.76	2.99	−3.61	−9.72	16.05	10.31	5.07	0.14	27.20	22.83	18.76	14.84	11.01
40	−31.56	−14.74	−22.60	0.91	−6.29	−13.00	15.19	8.80	2.93	−2.61	27.75	22.51	17.72	13.16	8.74
45	−36.02	−18.11	−26.52	−1.36	−9.12	−16.38	14.07	7.08	0.62	−5.49	27.88	21.92	16.47	11.30	6.33
50	−40.51	−21.56	−30.49	−3.77	−12.06	−19.85	12.73	5.18	−1.84	−8.47	27.20	21.01	15.03	9.30	3.80
75	−63.26	−39.81	−51.00	−17.47	−28.06	−38.15	3.64	−6.27	−15.65	−24.61	23.40	14.26	5.69	2.46	−10.28
100	−86.36	−59.12	−72.21	−32.97	−45.48	−57.48	−7.99	−19.87	−31.20	−42.09	15.70	4.53	−6.06	−16.20	−25.97

made, with the use of expression 12, by the Joint Computing Group, M.I.T. In Fig. 3, $W_{(J,M)}$ has been plotted. The small circles indicate the points at which the second-order
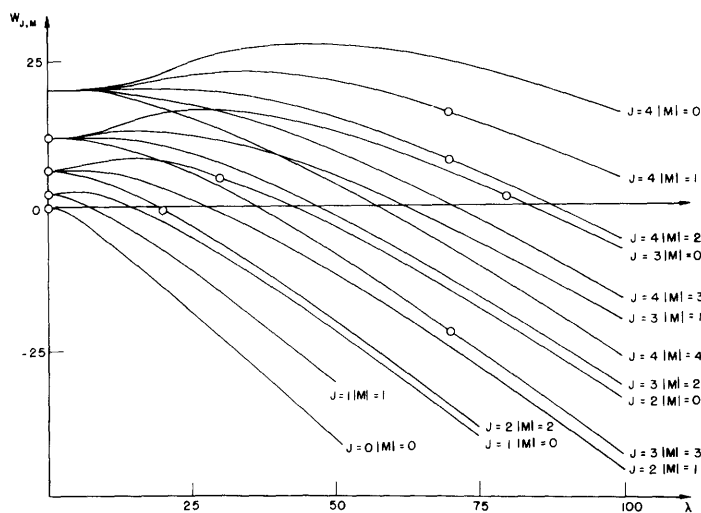

Fig. 3. High-field Stark effect in rigid linear rotors.

approximation, starting at λ = ∞, deviates from the true values by more than 0.1 unit, and thus its convergence properties are shown.

A vibrating-rotor approximation was also found for high-field Stark effect on the nonrigid linear rotor and the rigid asymmetric rotor.

2.2 AXIAL SELECTOR FOR ALKALI-HALIDE BEAM

We shall discuss a simple application of the calculations of section 2.1 — the axially symmetrical multipole focuser. In this type of focuser the field, and therefore the energy of a molecule in a given state, is a function of r only (see Fig. 4). In particular,
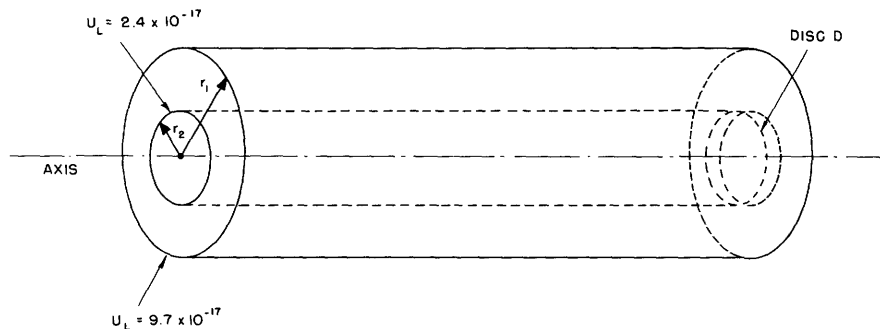
Fig. 4. Axial selector for alkali-halide beam.

let us look at the quadripole focuser, in which the field is proportional to m. Whether a molecule is trapped in, or escapes from, the focuser depends upon whether its initial energy U_I is below a limit U_L or not.

$$U_I = U_S(r_I) + \frac{Mv_{\perp I}^2}{2} \leq U_L \tag{15}$$

In particular, for $r_I = 0$, we find the maximum trapping angle:

$$Mv_{\perp I}^2 = 2U_L$$

$$\alpha = \frac{(v_{\perp I})_{max}}{\bar{v}} = \left(\frac{2U_L}{3kT}\right)^{1/2} \tag{16}$$

For sodium chloride, J = 2, M = 0, we find

$$U_L = 9.7 \times 10^{-17}$$

$$E_2 = 71 \text{ e.s.u.}$$

$$\alpha_{max} = 2.4 \text{ per cent}$$

If we make a long focuser with a small source, all of the molecules will move within a cylinder defined by $U_L = 9.7 \times 10^{-17}$. For the J = 1 state (see Fig. 3), the 1,1 state is completely divergent, whereas for M = 0 we find that

17

$$U_L = 2.4 \times 10^{-17} \qquad\qquad E_1 = 13 \text{ e.s.u.}$$

Therefore, if we place a disc, D, at the end of the focuser, we shall have selected only the J = 2 state, with an efficiency of approximately

$$\mathscr{E} = \frac{E_2^2 - E_1^2}{E_2^2} = 97 \text{ per cent}$$

On account of the small a_{max}, such a focuser would have to be very well collimated.

2.3 TRANSVERSE-ROD FOCUSERS

A study was performed on transverse-rod focusers in order to find an effective arrangement for state selection. The field in this type of focuser deflects particles in one plane only and not in a direction perpendicular to it. This feature raises the possibility of beam state selection with high directivity, which is important in high-precision spectroscopy. The fields of infinite rods can be calculated by using conformal mapping. The study can be simplified by assuming that the Stark energy is proportional to the square of the field strength, $W = a\xi^2$.

This assumption was admissible for ammonia with not too high fields. For alkali halides, the actual field dependence had to be used, and the trajectories had to be found by numerical integration.
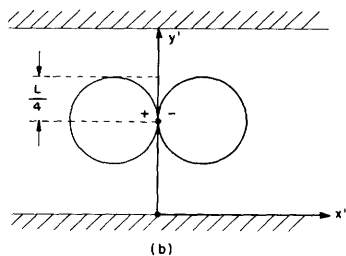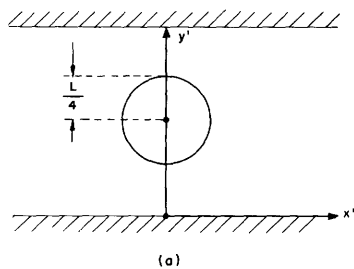

(a)

(b)

Fig. 5. Focusing-field configurations: (a) rod between two grounded plates; (b) two rods oppositely charged and touching.

The field of a rod between two grounded plates is (see Fig. 5a)

$$\phi = \phi_o \ln \frac{\cosh x + \sin y}{\cosh x - \sin y} \tag{17}$$

$$x = \frac{x' \pi}{L} \qquad\qquad y = \frac{y' \pi}{L}$$

For several rods, the potential

$$\phi = \Sigma \; \phi_i \ln \frac{\cosh (x - x_i) + \sin y}{\cosh (x - x_i) - \sin y} \tag{18}$$

gives a fair representation, but, in general, the rods will no longer be exactly circular. In the extreme case, with two rods oppositely charged and touching each other (see Fig. 5b), the potential is given approximately by

$$\phi \approx - 2\psi_o \frac{\sinh x \sin y}{\cosh^2 x - \sin^2 y} \tag{19}$$

We now define a potential U, with the property that the deflection angle $\beta(y)$ for a particle passing through the field in the x'-direction and at altitude y' is given by $\beta(y') = \dfrac{dU(y')}{dy'}$ for small angles.

For a single rod, we find that

$$\beta(y) = \frac{2}{W_o} \, a\phi_o^2 \left(\frac{\pi}{L}\right)^2 \frac{y \cos (2y) - \frac{1}{2} \sin (2y)}{\sin^2 (2y)} \tag{20}$$

and for the dipole, we find that

$$\beta(y) = \frac{2}{W_o} \, a\psi_o^2 \frac{\pi^2}{L^2} \left\{ \frac{-3[1 + \cos^2 (2y)]}{\sin^3 (2y)} + \frac{2y[\cos^2 (2y) + 5] \cos (2y)}{\sin^4 (2y)} \right\} \tag{21}$$

where W_o is the kinetic energy of the molecule.

Calculation for intermediary cases (two oppositely charged rods at varying distances) shows that the focuser becomes more effective when the two rods approach each other. Expressions 20 and 21 show that the deflection increases three times if the rods are moved from an infinite distance to the configuration of Fig. 5b. The closest approach is given by the maximum allowed field strength. Thus we decided to construct a focuser with several rods set at a distance L apart.

19

2.4 TRANSVERSE-ROD FOCUSER FOR SODIUM CHLORIDE

Let us now examine the focuser that was actually used. It consists of a lattice of rods alternately charged positive and negative. Figure 6 shows a cross section through the lattice. The white circles represent the alternately charged rods. The field

$$\phi = \sum_{0}^{7} \phi_i \ln \frac{\cosh (x - x_i) + \cos y}{\cosh (x - x_i) - \cos y} \tag{22}$$

was chosen, with $x_i = i\pi$. The field represents an infinite array of line charges of opposite polarity in the y-direction. The ϕ_i are so adjusted that the same absolute value of potential is given to all the rods. The potential does not fit exactly circular rods, but the deviations are small. For a rod potential of 20 kv, the trajectories for the relevant quantum states were calculated with the assistance of the Joint Computing Group, M.I.T. Figure 6 shows the trajectories for several quantum states; the aperture slits are shown on the right-hand side. The beam is followed back to the source and we see, for example, that only a small fraction of the molecules in quantum state J = 0, M = 0 passes through the aperture, the rest being held back because of the strong divergence of the beam. Almost the whole state J = 2, M = 2, however, passes through the aperture. The results are given in Table III. On the x-axis the points x_i, numbered 0 to 7, are taken. The y-axis is divided into 90 arbitrary units: −45 touches the surface of the rod below, and +45 the surface of the rod above. Several trajectories are calculated for each energy level J, M until a trajectory is found that just touches the aperture. Since the trajectories
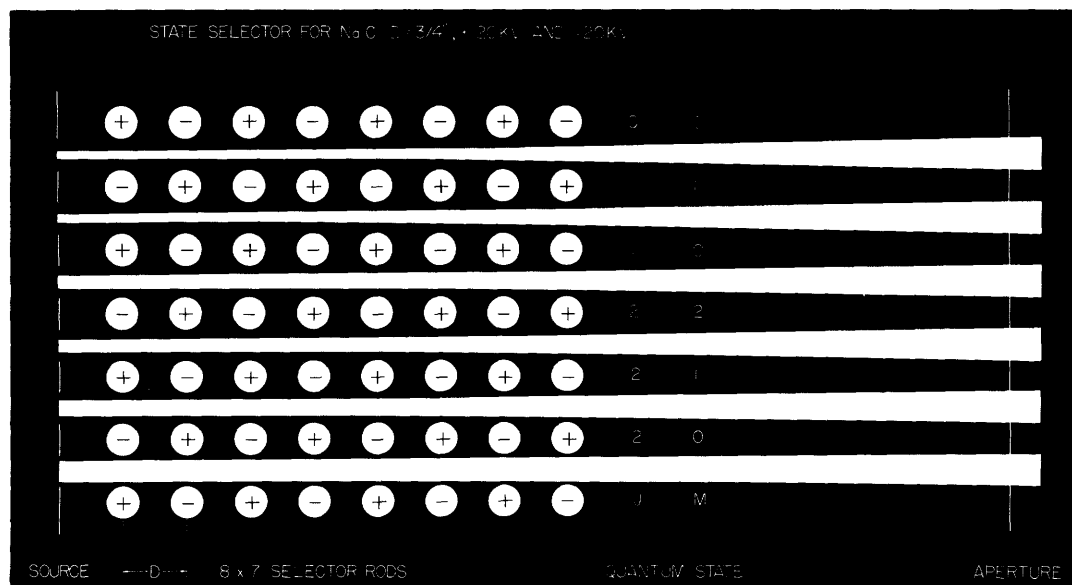

Fig. 6. Transverse-rod focuser trajectories.

are symmetrical about the x-axis, only positive y-values are plotted.

The calculation is correct for a given velocity and a beam that emerges strictly parallel. Actually, there will be a velocity spread. This was taken into account by inserting the factor 1/2 into the calculated selector efficiency. Furthermore, the beam is not strictly parallel. The influence of this fact on selector efficiency can be estimated from geometrical optics. We chose the principal plane (see Fig. 7) as the vertical symmetry plane of our focuser. For small deflections, the trajectory of the beam can then be idealized by a straight line that is refracted on the principal plane. A focal plane will only exist if the tangent of the angle of refraction is proportional to the distance from the horizontal symmetry plane. Reference to Table III shows that this condition is approximately fulfilled. A construction from geometrical optics shows (see Fig. 7) that we can compare the part of the beam selected by our aperture in the presence of a divergent lens with the part selected without it. The ratio of the selected refracted beam to the selected unrefracted beam is given by the area covered by the refracted beam in the oven aperture divided by the corresponding area in the unrefracted beam. We find that in case II a slightly less efficient selection takes place than in case I, whereas in case III the selection is very efficient because the refracted beam is entirely cut off. We therefore conclude that a small angular spread like that given by our actual source will not greatly impair the efficiency of state selection.

The focuser gives different population numbers not only for different J quantum numbers, but also within each J-state. This means that we shall find different populations for all of the different quantum states. It would be difficult to evaluate the populations exactly because the transitions among the M-levels occur easily in regions of small electric field. In the limit the transitions tend to equalize the populations within a given J-state, and therefore we have calculated the populations for the level with the assumption that this equalization takes place.
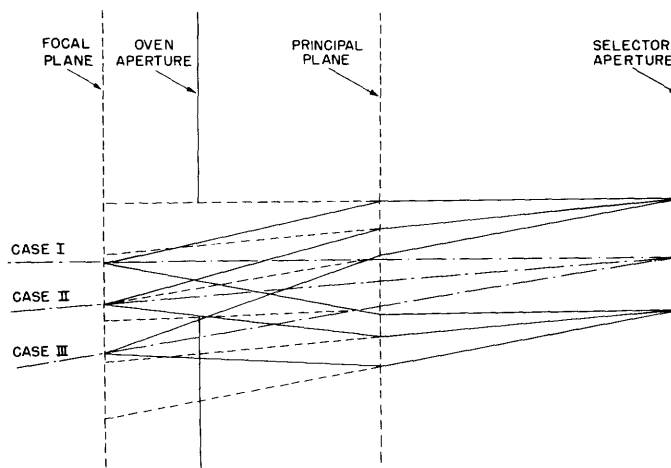

Fig. 7. Optical representation of state selector.

21

Table III. Trajectories of State Selector in Transverse Focuser.

J	M	x/y = 0	1	2	3	4	5	6	7	Aperture
0	0	5	5.1	5.4	6.0	6.9	8.1	9.6	11.5	27.8
		10	10.2	10.8	11.8	13.3	15.1	17.4	20.3	45.2
		9.9	10.1	10.7	11.7	13.2	15.0	17.3	20.2	45.0
1	1	10	10.2	10.6	11.3	12.3	13.7	15.4	17.5	35.5
		15	15.2	15.8	16.8	18.2	20.1	22.5	25.4	50.4
		20	20.3	21.1	22.40	24.2	26.6	29.7	33.50	65.6
		25	25.4	26.4	28.0	30.3	33.3	37.1	41.9	
		30	30.4	31.6	33.5	36.3	40.0	44.7	50.5	
1	0	10	10.1	10.3	10.6	11.0	11.5	12.1	12.8	18.9
		15	15.2	15.5	16.1	16.9	17.9	19.2	20.8	34.0
		20	20.2	20.7	21.5	22.7	24.3	26.3	28.7	49.0
		30	30.3	31.2	32.6	34.6	37.3	40.7	44.9	
		35	35.4	36.5	38.3	40.8	44.1	48.3		
		40	40.5	41.8	43.9	46.3				
		18.7	18.9	19.5	20.1	21.12	22.6	24.4	26.6	45.0
2	2	10	10.1	10.4	10.9	11.6	12.5	13.6	14.9	26.1
		15	15.2	15.6	16.3	17.3	18.6	20.2	22.2	39.1
		20	20.2	20.8	21.8	23.2	25.0	27.3	30.1	53.4
		17.1	17.3	17.7	18.6	19.7	21.2	23.1	25.5	45.0
2	1	10	10.1	10.2	10.4	10.7	11.1	11.5	12.0	16.40
		20	20.1	20.4	20.9	21.6	22.6	23.8	25.2	37.1
		25	25.2	25.7	26.4	27.4	28.8	30.5	32.6	49.8
		30	30.2	30.9	31.9	33.3	35.1	37.1	40.0	63.0
		35	35.3	36.1	37.3	39.1	41.4	44.3	47.9	
		40	40.4	41.4	43.0	45.2				
		23.1	23.3	23.7	24.3	25.2	26.5	28.0	29.8	45.0
2	0	10	10.0	10.0	9.9	9.9	9.9	9.8	9.7	8.8
		20	20.1	20.1	20.2	20.3	20.3	20.4	20.5	24.7
		30	30.1	30.4	30.8	31.3	32.0	32.8	33.8	42.2
		35	35.2	35.6	36.2	37.1	38.2	39.6	41.3	55.8
		40	40.3	40.9	41.8	43.1	44.8	46.9		
		31.0	31.2	31.5	31.9	32.5	33.3	34.2	35.3	45.0

22

The efficiency can be calculated as follows. The relative opening $Y_o/45$ gives the relative number, a, admitted in each state. Next, we calculate the average relative number, β, admitted in each J-level. The efficiency is obtained from the difference between the numbers, β, for $J = 1$ and $J = 2$, as follows.

State

J	M	a (%)	β (%)
0	0	22	22
1	1	29.4 ⎫	
1	0	41.5 ⎭	33
2	2	38.0 ⎫	
2	1	51.3 ⎬	49.5
2	0	69.0 ⎭	

If we take the factor 1/2 for the velocity distribution, we obtain the efficiency $1/2\ [\beta(J=2) - \beta(J=1)] = 8.2$ per cent.

2.5 NONADIABATIC LOSSES IN THE TRANSVERSE-ROD FOCUSER

As a molecule passes through our focuser, the electric field changes direction several times. Therefore the operating conditions must be such that the molecule will leave the focuser in the same state that it was in when it entered.

We have treated the molecule in the focuser as if time is only a parameter in the Hamiltonian. This treatment is known as the adiabatic approximation. If we consider a two-state system in which one state is initially unpopulated, we can show that the amplitude of the unpopulated state will be

$$|a_2| \approx \frac{\dfrac{E\mu}{\hbar_2}\,\omega}{\omega_{12}(\omega_{12} - \omega)}$$

Here, $\hbar\omega_{12}$ is the separation between the two states, and ω is the frequency of the perturbation. In our case, $|a_2| \approx 10^{-5}$; that is, the adiabatic condition is fulfilled.

In Fig. 3 we showed that two energy levels cross for certain values of the electric field. This means that ω_{12} goes through zero, and hence the adiabatic condition is no longer fulfilled. A special treatment is needed for this case, although there is reason to believe that not too many transitions occur — as long as the average energy separation along the trajectory is not small. For the sodium-chloride $J=2 \rightarrow J_1=1$ transition, proper adjustment of the electric field will obviate such a crossing.

The condition for adiabatic transition can also be obtained from the perturbation treatment that is customarily used in calculating transition probabilities in the presence

of periodic perturbations. However, certain conditions must be observed:

1. Since ω is less than ω_{12}, the "high-frequency terms" can no longer be neglected.

2. For a large perturbing field, the unperturbed states are mixed considerably as the field goes through its cycle. In order to determine whether or not a transition has occurred, the probability amplitudes before and after a complete cycle of the perturbing field must be compared.

Finally, we note that the perturbing field of the higher harmonics decreases as $(1/\cosh x)^n$, and hence that the influence of the harmonics becomes negligible for $x > 0$, $n > 1$.

III. MOLECULAR-BEAM MICROWAVE SPECTROSCOPE

3.1 DESIGN PARAMETERS

a. Qualitative Discussion

Dicke and Romer (22, 23) show that a gas of n particles radiates with an intensity of

$$I = I_o \frac{1}{2} n' \left(\frac{1}{2} n' + 1 \right) \tag{23}$$

if the n' particles are in a coherent state and I_o is the intensity for a single radiating particle. With a partition sum of 1/2, we find an emission of $I \approx n^2 I_o$, where n is the effective number of states.

The transition probability, ρ_ν, is given by Heitler (24) as

$$\frac{1}{\hbar^2} \rho_\nu |H'|^2 \tag{24}$$

For our cavity, it is given (25) by

$$\rho_\nu = \frac{2}{\pi} \frac{Q}{\nu} \tag{25}$$

$|H'|^2$, for dipole transitions, is equal to

$$\mu_{12}^2 \, 2\pi \, h\nu \, (n_\lambda + 1)/V \tag{26}$$

and hence, for $n_\lambda = 0$, we obtain

$$I = 8\pi \, \omega \, \mu_{12}^2 \, n^2 \, Q \, V \tag{27}$$

in which n is redefined as the particle density.

The necessary phase coherence can be established by pulses of suitable strength, or by preparing the beam in a separate cavity (23, 26).

The matrix elements for coherent induced emission are not proportional to n^2, but to n, because now transitions are induced in both directions. A typical experiment in stimulated emission will be analyzed in section 3.1b, and the emission will be

$$P_{signal} = \frac{32}{\pi^5} \, \omega \, V \, Q \, n^2 \, \mu_{ij}^2 \tag{28}$$

which is similar to the result obtained for spontaneous coherent emission. The factors are different: the second experiment is actually realizable; but in the first experiment only the theoretical limit is given. In an actual experiment, but with high pulse repetition rate, Dicke and Romer (23) obtained the factor $\pi/4$.

A special case arises when the signal emitted is sufficient to stimulate further

emission. This occurs in maser oscillation, and thus the electric field E has to be strong enough to flip the molecule during the relaxation time. That this condition is closely related to the condition that the energy released by the molecules must exceed the energy absorbed in the cavity has been shown by Shimoda, Wang, and Townes (27).

It has been shown by Johnson and Strandberg (28) that the condition for a complete flip is

$$\frac{E \mu_{ij} \tau}{2\hbar} = \frac{\pi}{2} \tag{29}$$

This means that power loss to the cavity can be written in these two equivalent forms:

$$P_o = \frac{\omega}{Q} \frac{E^2}{8\pi} V = \frac{\omega}{Q} \frac{h^2 V}{32\pi \mu_{ij}^2 \tau^2} \tag{30}$$

$$P_o = \frac{1}{\tau} nVh\nu$$

With $\tau = L/\overline{v}$, we obtain

$$n = \frac{h\overline{v}}{16\mu_{ij}^2 L Q} \tag{31}$$

Approximately the same result could have been obtained by using the concept of induced emission with a transition probability of $\overline{v}/L$. The radiation density is calculated by assuming that all of the radiation is concentrated within the spectral width of the stimulating radiation. The photon density is found to be $n_\lambda = nV$. Hence

$$n = \frac{h\overline{v}}{32\pi^2 \mu_{ij}^2 L Q} \tag{32}$$

Equation 32 is the equivalent of Eq. 31 except for an error in the numerical factor that arises in using small-signal theory.

Finally, note that the condition that coherent spontaneous emission just flips the molecules during the relaxation time leads, again, to

$$\frac{16\pi \omega \mu_{ij}^2 n^2 Q}{h\nu V} = \frac{n}{\tau}$$

or to

$$n = \frac{h\overline{v}}{32\pi^2 \mu_{ij}^2 Q L}$$

This indicates that in addition to incoherent spontaneous emission, which has been treated by Strandberg (25), coherent spontaneous emission (molecular ringing) plays

an important role in maser processes.

b. Signal-to-Noise Ratio for Stimulated Emission

We shall now discuss the signal power produced by an apparatus similar to the Stark microwave spectroscope, of which Strandberg (4) has given an analysis.

The periodically applied Stark effect modulates the microwave power with a modulation index $m = \gamma/\pi$, where γ is the relative change in power with absorption. This gives $P_{signal} = P_o(m^2/2)$. However, since $P_{abs}/P_o = \gamma$, we obtain $P_{signal} = P_{abs}^2/2\pi^2 P_o$. In a bridge system with no Stark modulation, it can be shown that P_{signal} is larger by a factor $(\pi/2)^2$. This factor is the result of the fact that in the Stark system the higher harmonics of the square wave are neglected.

When an observation is made without a bridge, the signal power is larger, but so is the noise power; and the signal-to-noise ratio is the same, within a factor of 2, as Townes and Geschwind (29) have shown.

With our beam, for the signal-to-noise ratio, r, we obtain

$$r = \left(\frac{P_{abs}^2}{2\pi^2 P_o \, kT \, \eta \, B}\right)^{1/2} \tag{33}$$

in which $P_{abs} = A \, n\bar{v} \, h\nu$, where $n\bar{v}$ is the beam density multiplied by the properly averaged beam velocity. From several representative velocities, we chose the most probable velocity:

$$\bar{v} = \left(\frac{3kT}{m}\right)^{1/2} = 5.9 \times 10^4 \tag{34}$$

for sodium chloride. P_o is the power required for producing the transitions for observation. The transition condition is given by Eq. 29, and we have

$$P_o = \frac{\omega}{Q} \frac{\bar{v}^2 \, h^2 \, V\pi}{256 \, \mu_{ij}^2 \, L^2}$$

for the $TE_{17,0,1}$ mode, and hence

$$P_{signal} = \frac{32}{\pi^5} \omega \, V \, Q \, n^2 \, \mu_{ij}^2$$

which is the result obtained in Eq. 28

c. Application to the Molecular-Beam Microwave Spectroscope

The density of particles in the beam, n, has to be evaluated. This will be done in two steps. First, n will be obtained for a beam without a state selector. Second, the effect of the state selector will be considered. The beam is formed from a cloud of density, N, inside the evaporating oven. If the beam is given a linear aperture angle γ,

then the fraction selected is $\gamma^2/4$; with 50 per cent transparency we have a density of $n_t = N\gamma^2/8$. This argument holds only if N is small enough and the mean-free path λ is large enough to permit free passage of the beam through the effuser channels of length ℓ.

$$\lambda = \frac{1}{b^2 \pi N} > \ell \tag{35}$$

Typical values are:

$\ell = 1$ cm

$b = 4$ A

$N = \frac{10^{16}}{16\pi} \approx 2 \times 10^{14}/cm^3$

$n_t' = 1.25 \times 10^{-5} N = 2.5 \times 10^9/cm^3.$

At this point, we introduce an additional factor of $1/\sqrt{2}$ to account for the fact that the n_t' molecules are emerging with a velocity spread, instead of being monoenergetic. Thus, we have $n_t' = 1.8 \times 10^9/cm^3$. Now, a factor b must be introduced to account for the fact that no state selector is used. This means that the upper and lower states of our transition are almost equally populated. Their energy difference causes only a small population difference, the ratio of the population of the upper state to the population of the lower state being $\exp(-h\nu/kT)$. Hence, we have $\exp(-h\nu/kT) - 1 \approx h\nu/kT$. With the definition

$$b = \frac{h\nu}{kT} \tag{36}$$

for our sodium-chloride transition,

$$b = \frac{6.62 \times 10^{27} \times 2.6 \times 10^{10}}{1.38 \times 10^{16} \times 828} = 1.5 \times 10^{-3}$$

Summarizing, we have

$$P_{signal} = \frac{32}{\pi^5} \omega V Q \mu^2 I n^2 = \frac{32}{\pi^5} n_t^2 f^2 I \mu^2 \omega V Q b^2$$

where, for our sodium-chloride transition, we have

μ	$= 8.5 \times 10^{-18}$ e.s.u.	molecular dipole moment
I	$= 9.2$	intensity
f	$= 8.4 \times 10^{-6}$	partition sum
n_t	$= 1.8 \times 10^9$	beam density
b	$= 1.5 \times 10^{-3}$	Boltzmann factor
ω	$= 2\pi\nu = 1.63 \times 10^{11}$	frequency
Q	$= 7.10^3$ cm^3	quality factor of cavity
P_{signal}	$= 1.8 \times 10^{-13}$ erg/sec	signal power.

28

The signal power has to be greater than the noise power in the system. Ideally, the noise power equals the available thermal noise power; that is, P_{noise} = kTB, where B is the bandwidth of the system. In our case, B is the output bandwidth or, since we use an RC filter with a time constant τ, we have B = $1/2\tau$. In reality, a noise figure η must be introduced. With η = 13 db, and τ = 3 sec, we obtain a signal-to-noise ratio, r, of 1.4. (In Section II, we saw that the state selector has an efficiency of 8.2 per cent; hence we multiply r by $\frac{8.2}{0.15}$ and obtain r_s = 80.)

Now we shall calculate the analogous results for ammonia. From the data of our system, we find

$$f = \frac{1}{3400}$$

$$I = 410$$

$$b = 3.8 \times 10^{-3}$$

$$\omega = 1.5 \times 10^{11}$$

$$\mu_o = 1.5 \times 10^{-18}$$

$$\bar{v} = 7.1 \times 10^4$$

and hence r = 115. The beam and cavity with 10 per cent efficiency in the state selector would produce r'' = 3000. Our calculation suggests that the efficiency of NH_3 is approximately $(3000/80)^2$, or 1300 times as effective as NaCl. This large difference is attributable in part to the fact that a great number of accidental degeneracies that were incorporated in the calculations for NH_3 were not taken into account in the data for NaCl because we did not know its spectrum well enough.

d. Conditions for Maser Operation

It is of interest to calculate the Q_{min} required for making the large beam self-oscillating. In this calculation the flip condition stated in section 3.1a must be fulfilled by the field created by the flipping molecules. This means that

$$\frac{\omega \bar{v}^2 h^2 A}{32\pi\gamma_o^2 \mu^2 L Q} = nh\nu A \bar{v}d$$

where d represents the accidental and M_F-degeneracy. We then obtain

$$n = \frac{h\nu}{K(F, F')/16\mu^2 I L Q}$$

which, for n = $\frac{1}{10} n_t$ f = 5×10^4 per cm^3, gives Q_{min} = 42,000 for ammonia. For a cavity of the size of ours, the realization of such a Q does not appear to be impossible.

29

However, a Q of 5000 would be sufficient for a state selector that is 100 per cent efficient.

Note also that in the conditions stated above the cavity cross section did not appear. This suggests that a precision device could be made with a much narrower, but equally long, cavity. The output power would be lowered in proportion to the cross-section area.

The flip condition can also be applied to sodium chloride, and we have $Q_{min} = 3 \times 10^5$. For maser operation, we find that NaCl is 80 times less effective than NH_3, the reason being that, whereas the difference in dipole moment is still favorable to NaCl, the difference in partition and degeneracy appears in the first order. A Q_{min} of 30,000 is needed if we decrease the length by a factor of 10 and increase the flux by 1000, which can be achieved by reducing the aspect ratio by a factor of 10. This means that an ordinary sodium-chloride maser should be feasible, even if a focusing structure like ours is used.

However, with the help of Stark energies (11, 12) different focusers can be designed. The designer should not limit his choice to the designs that are already known but should look for the most effective design for his particular task. In a spectroscope the signal power will increase proportionally with frequency. The field in the focuser will also rise proportionally with frequency. However, at sufficiently high frequencies the focuser is no longer needed, since the thermal-equilibrium distribution provides for a better population difference.

Since the frequency does not appear in the oscillation condition, masers of lower frequency appear to be feasible. We find that if one alkali halide is successfully observed, the others can also be observed. The beam flux can be varied by diminishing the effuser channel length, ℓ. The flux will be limited by consideration of the running time of the device. However, in no case will n_t be allowed to become large enough to produce a transition of the selected state in the focuser or in the cavity. For sodium chloride, this limits us to $n_t < 2 \times 10^{11}/cm^3$.

e. Precision

The precision of measurement is determined by the width of an emission line. The long cavity of our system gives a total linewidth of $\Delta \nu_L = 1$ kc, which, according to information theory (13), amounts to a statistical precision of

$$P = r \frac{\nu}{\Delta \nu_L} = 1.7 \times 10^9 \tag{37}$$

or six parts in 10^{10}. This accuracy might be impaired by pulling effects. The part of the pulling that is caused by the cavity setting is given, approximately, by

$$d\nu \approx \frac{\Delta \nu_L}{\Delta \nu_c} \delta \nu \tag{38}$$

where $\Delta \nu_c = \nu/2Q$, and $\delta \nu$ is the error in cavity setting (6). In order for this error not

to exceed the readout error, we must have $\delta\nu = \pm 150$ kc/sec. A time constant one hundred times longer (300 sec), such as is used in atomic clocks, would produce an absolute accuracy of six parts in 10^{11} and require a cavity setting that is better than 15 kc.

3.2 EXPERIMENTAL APPARATUS

a. Electronic System

Figures 8 and 9 illustrate the present status of the molecular-beam microwave spectroscope. Figure 8 is a block diagram of the electronic system. Figure 9 shows the auxiliary apparatus. A system of relays provides protection against damage in case of vacuum breakdown.

The spectroscope is of the resonant-cavity type and uses two bridges — one for the carrier and one for the local oscillator. The system operation is described below. The beam source, the interaction cavity, and the frequency control system which had to be developed especially for this spectroscope, are described in the following sections.

The power level of the signal is controlled (see Fig. 8) by setting attenuator 1 so that the crystal produces a specified current (50 μa). Calibrated attenuators 2 and 3 are set to reduce the power level to the required value of 4.5×10^{-10} watt. Care had to be taken to reduce the pickup of the signal radiated by the signal klystron. Steel wool wrapped on waveguide joints is quite effective in isolating this radiation. The power setting is cross-checked by comparing the power with the background noise after this noise has been measured quantitatively by means of a gas-discharge noise source (Roger White Model GNW-K_2-18). The noise could have been measured more precisely with a K-band isolator between source and receiver, since some modulation of the local oscillator could have occurred. Our measurements without the isolator gave a noise figure of 13 db.

We tried to balance out, by using a balanced mixer, the additional noise that might be introduced by the local oscillator. Crystals also show excess noise at low frequencies. Our detection at 30 mc should be outside the excess-noise region. However, the rf carrier of the 300-cps signal may beat with the excess-noise components to give excess noise by double conversion. Hence, we suppress the carrier. A small 30-mc signal, modulated at 300 cps and weakly coupled to the i-f input, can be observed with the microwave bridge operating at different rf levels. The required amount of carrier suppression can be determined by noting the point where the rf carrier increases the signal-to-noise ratio of the injected 300-cps signal.

The weak signal power is detected, in the most efficient way; that is, by a linear system. The ammonia maser detects the emitted power in a partially nonlinear process, which means that the output bandwidth is the geometrical mean of the bandwidth of the final filter and the i-f bandwidth. In our case, the final filter alone determines the bandwidth. This is achieved by applying Stark modulation to the molecular beam. The frequency of the modulation is determined by two conditions:
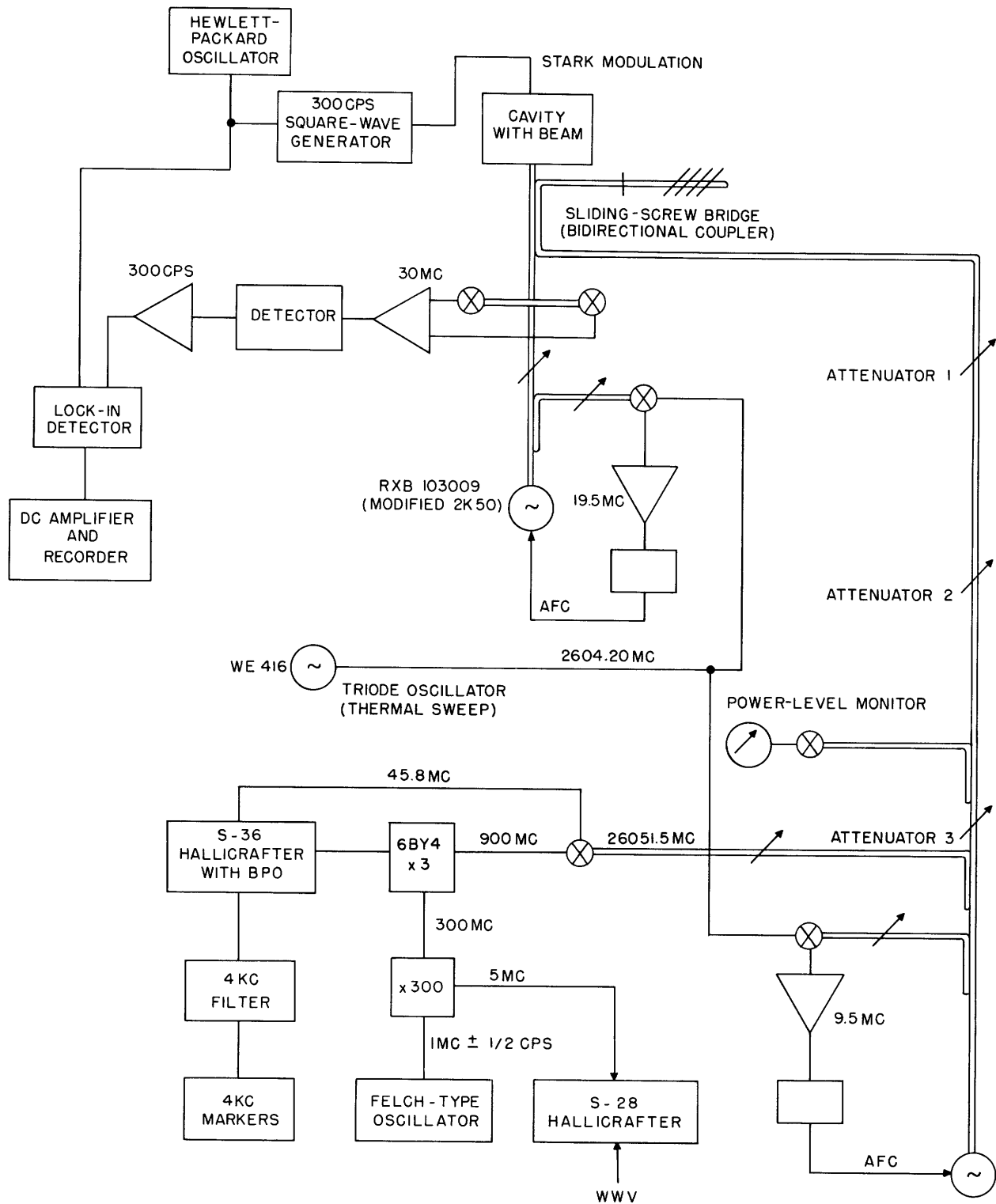
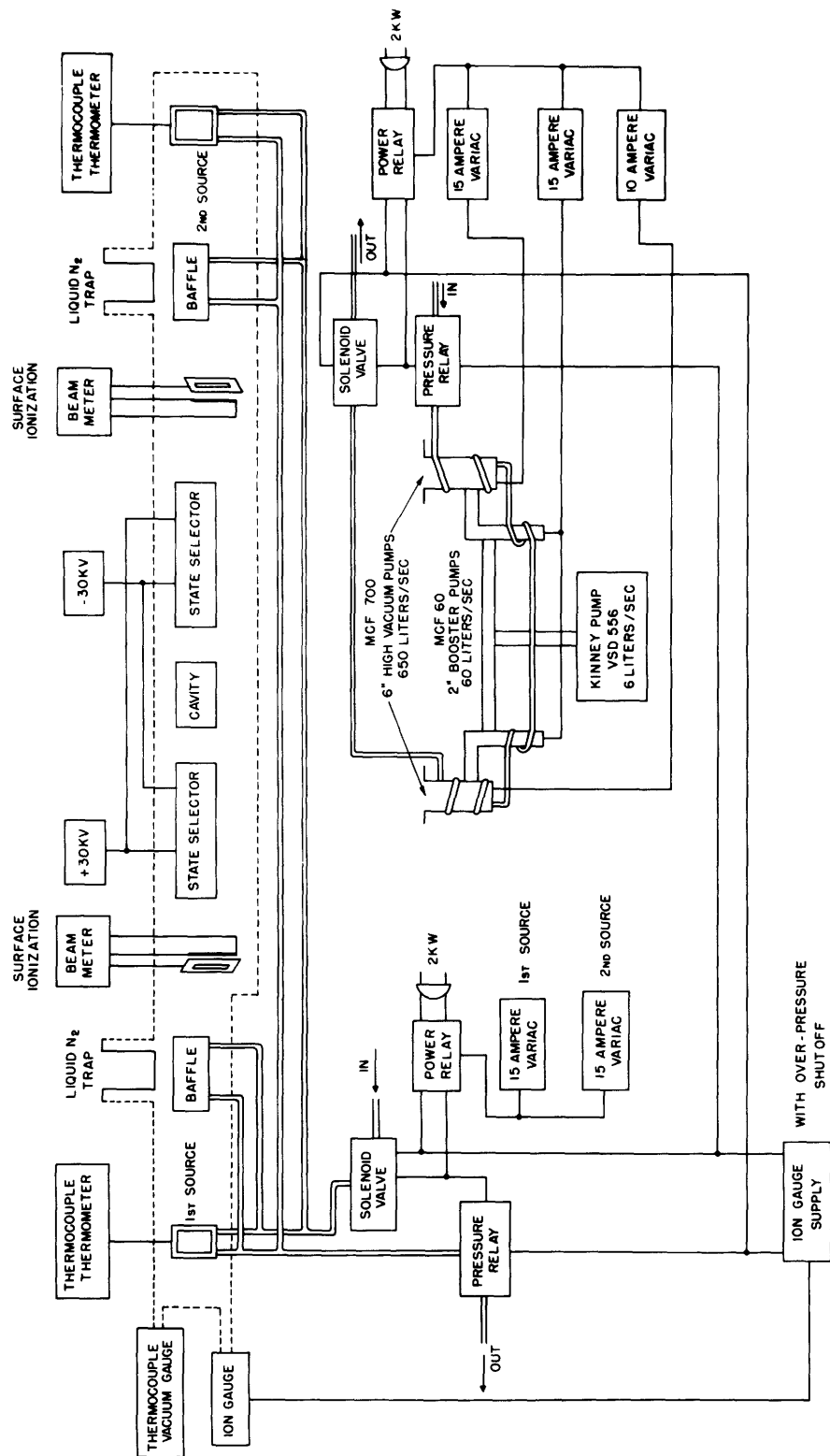Fig. 8. Molecular-beam microwave spectroscope.

Fig. 9. Auxiliary apparatus for molecular-beam microwave spectroscope.

33

1. The modulation must be slow compared with the transit time of the beam.

2. The modulation frequency must be as high as is compatible with the first condition, in order to minimize excess noise in the receiver crystal.

If the first condition is violated, we no longer obtain modulated emission but, rather, unmodulated emission at several frequencies (4). It is essential in the construction of a high-precision spectroscope that an electromagnetic radiation field, whose properties are well controlled in space and time, be available. The stability requirements can be summarized by the three following conditions:

$$\left.\begin{array}{c} 4\bar{v}/L\Delta\beta < \Delta\nu \\ \bar{v}/L < \Delta\nu \\ \delta\nu < \Delta\nu \end{array}\right\} \tag{39}$$

where $\Delta\beta$ is the angular spread of the particles in the y-direction; L is the length of uniform phase in the cavity; $\delta\nu$ is the spectral width of the source used for observation; and $\Delta\nu$ is the spectral width of the line that will be observed. The first condition requires a well-collimated source; the second, a large cavity; and the third, a stable frequency source. The work which was done to satisfy these three conditions will now be described.

b. Beam Source and Beam Detector

A schematic diagram of the beam-source assembly is shown in Fig. 10. The oven housing was of stainless steel, the actual collimator was of corrugated nickel ribbon, as described by Strandberg and Dreicer (1). [Details of the oven construction are given in RLE drawings Nos. A-1642B, A-1642C, B-1642D, B-1642E, and B-1642F.] The oven was run at a temperature of 845° K. The function of the oven is to produce vapor of molecular sodium chloride of sufficient pressure to supply a beam of required strength.

Two disturbing influences have to be mentioned: polymerization will create a fraction of $(NaCl)_2$ molecules. A dimerization of potassium chloride up to 15 per cent for an oven pressure of 50 microns is quoted by Datz and Taylor (30). Miller and Kusch (31) mention that polymerization should increase with oven temperature. The oven pressure used in our experiment was 1.5 microns. We therefore do not expect dimerization to be significant.

Furthermore, the effect of surface ionization has to be considered. This effect is governed by the Saha-Langmuir equation

$$\frac{n_+}{n_a} = \left(\frac{1 - r_+}{1 - r_a}\right) \frac{\omega_+}{\omega_a} \exp\left[\frac{e(\phi - I)}{k\Gamma}\right] \tag{40}$$

where r_+ and r_a are the reflection coefficients for ions and atoms; $\omega_+/\omega_a = 1/2$; I is the ionization potential; and ϕ is the work function. Equation 40 was carefully studied by Datz and Taylor (30) for alkali halides on tungsten. From their investigation we find that at temperatures of 1100° K, the Saha-Langmuir equation is fulfilled for tungsten if
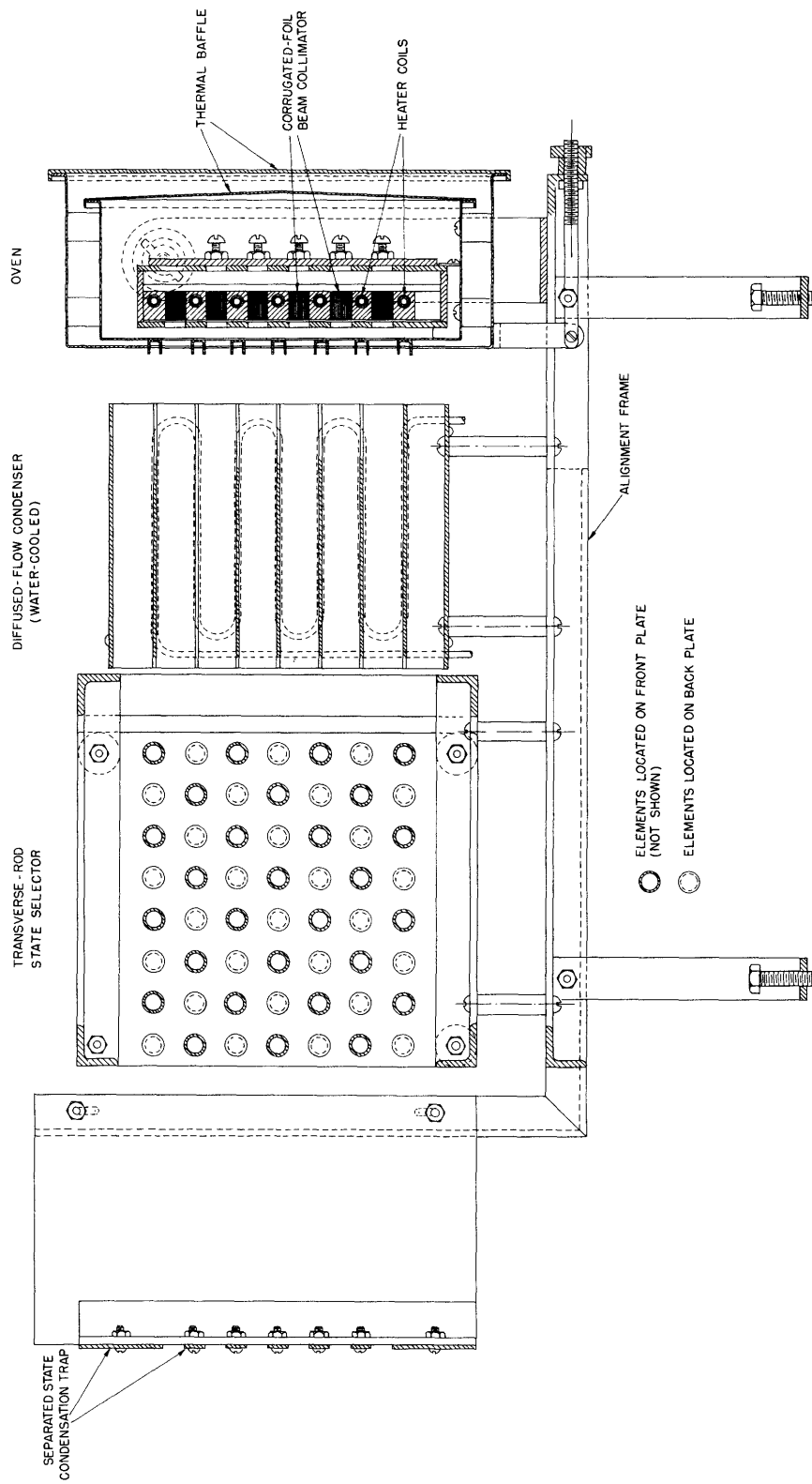
Fig. 10. Cross section of oven, shield, baffle, and selector.

THERMAL BAFFLE

CORRUGATED-FOIL
BEAM COLLIMATOR

HEATER COILS

OVEN

ALIGNMENT FRAME

DIFFUSED-FLOW CONDENSER
(WATER-COOLED)

TRANSVERSE-ROD
STATE SELECTOR

ELEMENTS LOCATED ON FRONT PLATE
(NOT SHOWN)

ELEMENTS LOCATED ON BACK PLATE

SEPARATED STATE
CONDENSATION TRAP

the ionization coefficient of the alkali metal is used. The ionization efficiency is slightly increased for the halides, possibly because of formation of a partial halide film. For platinum, the efficiency is strongly decreased, possibly because of strong reflection of the molecules. In all cases, ionization practically ceases below 1100° K. This can be explained by a lowering of the work function that is caused by surface contamination. If this result, which was found for tungsten and platinum, can be applied to steel and nickel, then we should not expect the oven to ionize sodium chloride. If some ionization should occur, the ions will probably not penetrate the focuser because strong image forces will be acting. The lateral displacement is $\Delta s \approx \dfrac{e^2}{kT\gamma^2}$, where γ is the aperture angle; or $\Delta s \approx 0.01$ inch in our geometry. The measurements by Datz and Taylor indicate that 83 per cent of the incident potassium-chloride molecules should be ionized on a tungsten filament at a temperature of 1500° K. This is essentially the same ionization efficiency as that measured for atomic potassium. Atomic sodium is ionized at 2000° K with only 5 per cent efficiency. This is to be expected from the higher ionization potential of sodium. The efficiency for potassium decreases with temperature; the efficiency for sodium increases. Tungsten oxide has a higher work function than tungsten, and therefore it produces a 100 per cent efficient ionization for both potassium chloride and sodium chloride. This explains the confusing observation that the sodium-chloride beam strength, as measured with an ionization detector, decreases with operating time. Actually, the beam is constant, but the hot filament becomes progressively deoxydized. While the ionization detector was valuable as a monitor of the time dependence of the beam, the condensation target provided information about the spatial distribution of the beam.

c. Interaction Cavity

The construction of a large cavity that can be excited in a well-determined resonant mode is of double interest for beam spectroscopy. On the one hand, the extension of the cavity dimensions will allow higher precision in measurements because of longer interaction times. On the other hand, once the technique of building cavities that are large compared with the wavelength is advanced, the restriction on cavity Q for high frequencies might be overcome and the generation of submillimeter waves might be possible.

Our cavity (see Fig. 11) with axes a, b, d was excited in the $TE_{17, 0, 1}$ mode. The mode was drawn from the ordinary $TE_{1, 0}$ mode waveguide by means of the collimating system shown in Fig. 12. The $TE_{1, 0}$ mode is fed into a "pillbox antenna" (32) and goes from there into a horn and a cylindrical plexiglas lens. The large coupling surface ensures that only the desired mode has an appropriate external Q, to allow proper loading. Additional mode control is exercised by means of damping slits, D, in the top and bottom surfaces, and by the fact that the two end surfaces are open in order to permit the entrance of the two beams.

The inner dimensions of the cavity are: a = 3.85 inches, b = 5 inches, d = 28 inches. It has a loaded Q of 5000 and is critically coupled to the input. The distributed iris
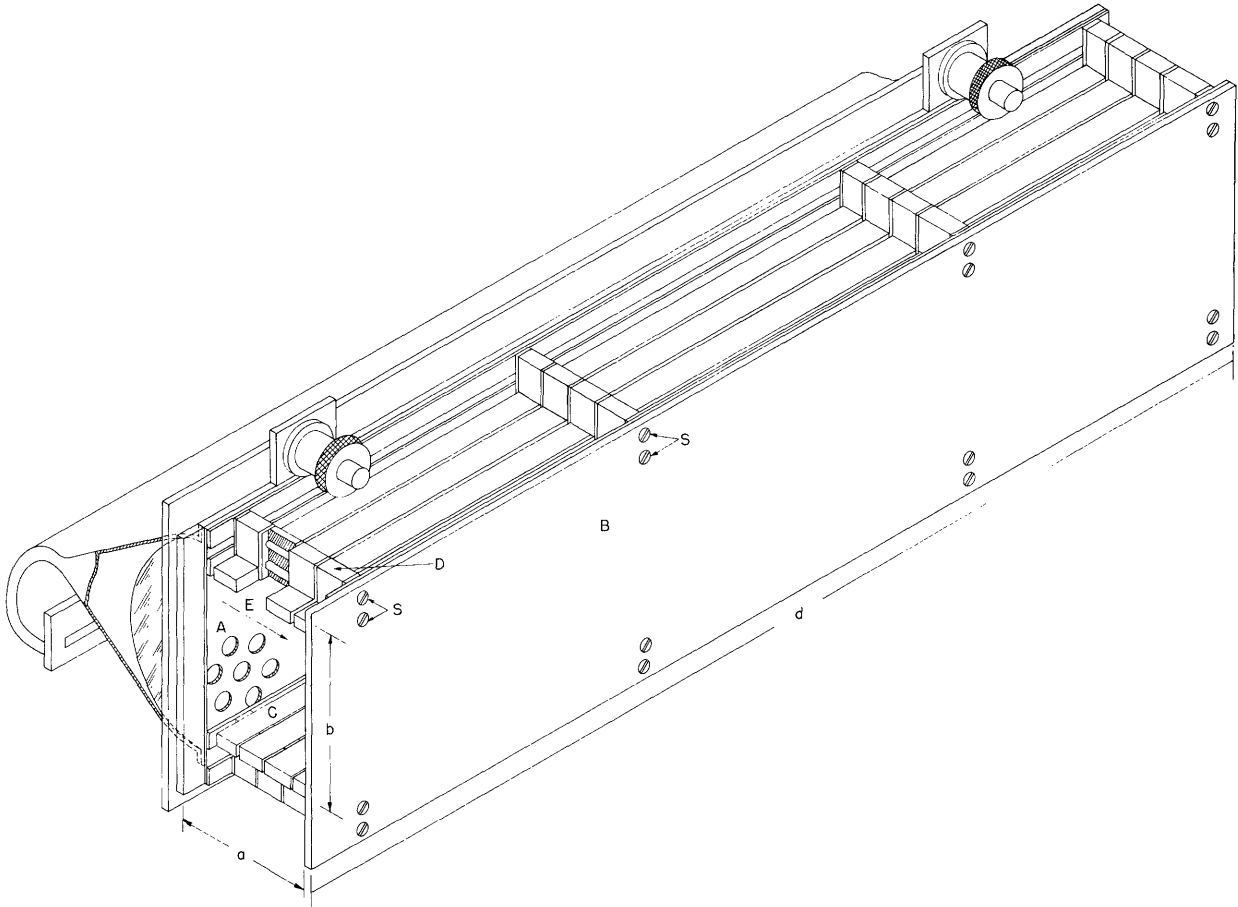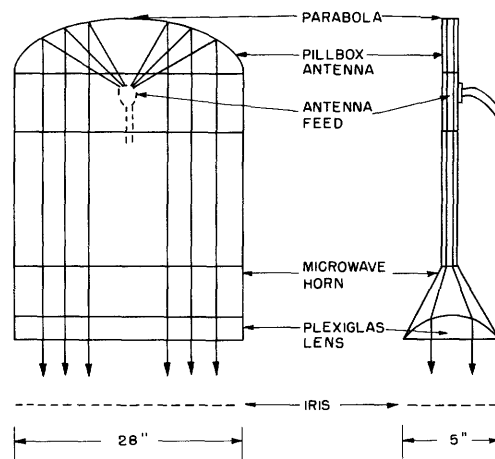
Fig. 11.   Large mode-controlled cavity.

Fig. 12.   Mode-control system.

consists of a copper-plated perforated steel plate, 1/16 inch thick, with 3/16-inch round holes, whose centers are 5/16 inch apart and staggered. The neoprene spacers in the damping slits can be compressed by the mounting screws, S, and thus a tuning range of 0.05 per cent is obtained. Across the side surfaces, A and B, a homogeneous electric field, E, can be applied for Stark modulation, since the bars, C, are isolated.

This cavity showed only one strong mode every 100 mc. This is remarkably selective action as compared with the natural-mode density of such a cavity, which is obtained as follows.

The number of modes in the cavity is determined by the condition

$$\ell\lambda_1 = 2a \qquad\qquad m\lambda_2 = 2b \qquad\qquad n\lambda_3 = 2d$$

The frequency is

$$\nu^2 = \frac{c^2}{\lambda^2} = c^2\left(\frac{1}{\lambda_1^2} + \frac{1}{\lambda_2^2} + \frac{1}{\lambda_3^2}\right) = \frac{c^2}{4}\left[\frac{\ell^2}{a^2} + \frac{m^2}{b^2} + \frac{n^2}{d^2}\right]$$

The number of modes with $\nu < \nu_o$ is

$$N = \left(\frac{8\pi}{3}\right)(abd)\left(\frac{\nu^3}{c^3}\right)$$

$$\frac{dN}{d\nu} = \left(\frac{8\pi V}{\lambda^3 \nu_o}\right)$$

(41)

which yields $\dfrac{dN}{d\nu} = 4.5/\text{mc}$. The reduction is seen to be approximately five hundredfold.

d. Ultrastable Frequency Sources

Figure 8 shows the use of the stable sources in our experiment. A planar triode oscillator for operation at 2604.20 mc, similar to the one described by Rearwin (33), was built. A tuning screw on the grid cavity produced tunability over one part per thousand. The signal oscillator and local oscillator were locked to this cavity by means of high-gain automatic-frequency-control loops. The stable K-band signal was then compared with the output of a frequency multiplier chain consisting of a 1-mc oscillator and frequency multipliers to 26,100 mc. The beat with the desired signal of 26,051.5 mc was monitored against a Hallicrafter beat frequency oscillator. The stability of ± 200 cps that was achieved was considered marginal but sufficient for experimentation. An audible beat note was obtained at K-band.

A readily tunable discriminator was used in the frequency stabilizing loop (see Fig. 13). In a simple analysis the detector crystals X_1, X_2 can be replaced by C_{eq}. The input is connected to a dc grounded source whose impedance is high compared with $1/\omega C_{eq}$. For example, the input might be connected to the output of a double-tuned filter. The capacitors C_3, C_4, and C_5 are large rf admittances. The input is then divided between two impedances:

38

$$Z_1 = \frac{1}{i\omega C_{eq}} \qquad\qquad Z_2 = \frac{1}{i\omega C_{eq}} + \frac{i\omega}{C(\omega_1^2 - \omega_2^2)}$$

If $\omega = \omega_1$, then $Z_2 = \infty$, and the current, i, flows entirely in X_1, creating the positive peak shown in Fig. 14. The negative peak appears when i is flowing entirely through X_2; that is, when $Z_2(\omega_2) = 0$; from which we find

$$\omega_1 = \frac{1}{(LC)^{1/2}} \qquad\qquad \frac{\omega_1 - \omega_2}{\omega_1} \approx \frac{C_{eq}}{2C}$$

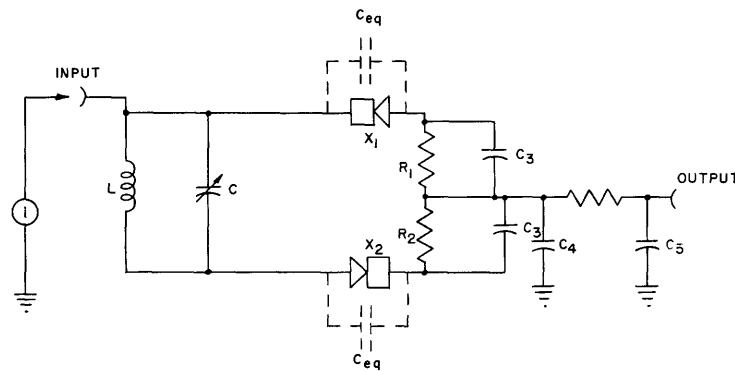The circuit is similar to the Weiss discriminator, described by R. V. Pound (34).
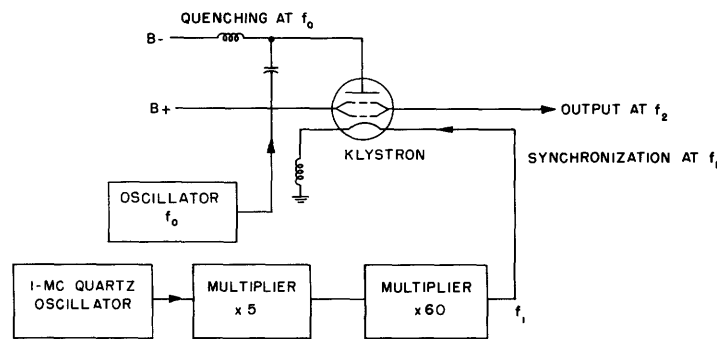

Fig. 13. Frequency discriminator.

Fig. 14. Block diagram of phase-locking system.

The application of phase-locking techniques to K-band precision measurements was studied. The power needed for stimulation of our cavity was found to be $p = 4.10^{-10}$ watt. It has been shown (35) that a phase-locked signal will produce an off-carrier noise per cycle which is theoretically approximately 10^{10} times below carrier noise. By matching the cavity and bridging the stimulating signal, the off-carrier noise can be reduced an

39

additional 30 db, or to 20 db below thermal noise.

Figure 14 is a block diagram of the phase-locking scheme that uses superregenerative amplification (36). The klystron is periodically quenched out of oscillation (by frequency f_o), and the incipient oscillation of each new pulse is synchronized by an applied frequency, f_1. The output of the klystron consists of a multiple of f_1 plus or minus a number of sidebands, separated by f_o; that is, $f_2 = n f_1 \pm m f_o$. It can be seen that this scheme also incorporates an easy and efficient means of obtaining a microwave-frequency signal (f_2) which is offset by a variable amount (through the variation of f_o) from a high harmonic of a stable low-frequency reference signal (f_1). The outstanding feature of the new phase-locking apparatus appears to be its extreme reliability over long periods, even under severe environmental conditions. Since the quench frequency f_o and the reference frequency f_1 are not harmonically related — a condition not previously contemplated (for example, see ref. 36) — we have introduced a means of offsetting the klystron frequency from the reference frequency in a readily controllable manner.

Application of our earlier phase-locking technique (35) could be made by using a sodium-chloride maser as a standard and transferring its frequency to our signal oscillator.

e. Experimental Results

The final result of this work will be the measurement of hyperfine spectra of some of the alkali halides; this work has not yet been carried out.

The experimental results reported here will give an insight into the progress of our project and should be helpful in future work.

1. Beam System

Oven pressure, 1.5×10^{-3} mm Hg

Oven temperature, 848° K

Heating power per oven, 600 watts

Beam strength:

Measured by surface ionization, 7.7×10^{15} particles/sec

Measured by condensation target, 2.4×10^{15} particles/sec

Calculated from measured oven temperature, 6×10^{15} particles/sec

Maximum beam current (for absorption experiment), 10^{17} particles/sec

Vacuum (mm Hg):

Fore vacuum, 5×10^{-2}

High vacuum, 3×10^{-6}

High-vacuum liquid N_2, 1.4×10^{-7}

High vacuum with oven running, 2×10^{-6}

A condensation target was utilized for studies of beam collimation. Figure 15 shows two cross sections through the beam. The dark (dotted) rings correspond to a given amount of deposited beam material. On the right-hand side, two rings (R) appear,
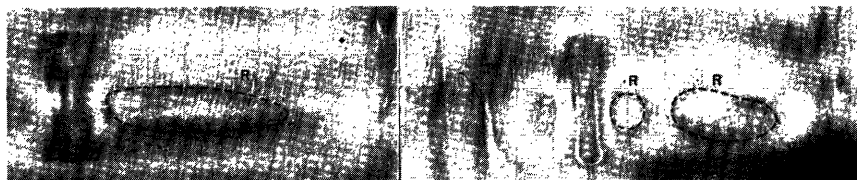
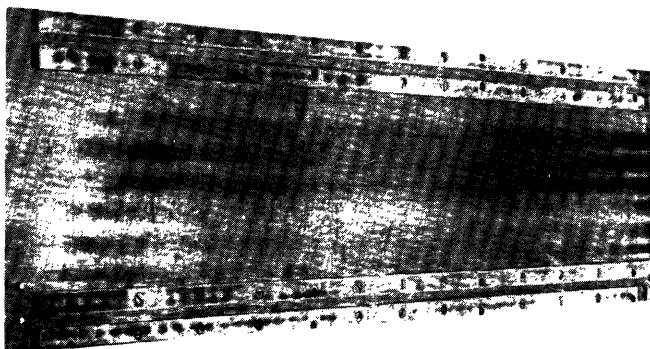Fig. 15. Study of alkali-halide beam collimation.

Fig. 16. Trace of sodium-chloride beam on cavity wall.

indicating an uneven beam distribution. On the left-hand side, only one ring (R) is found, indicating better collimation.

A longitudinal section through the beam in the interaction space is seen on the condensation target shown in Fig. 16. It is simply the back wall of the interaction cavity. The six black lines are created by the 12 molecular beams injected from the two sources.

2. Electrical System

The noise figure (measured with Roger White Model GNW-K_2-18 noise source) was 13 db. The spectral width of the exciting signal can be estimated, from the width of the markers in Fig. 17, to be approximately 200 cps. Figure 18 shows a 500-cps beat between two X-band signals that are phase-stabilized to two different quartz-crystal tuned oscillators. The frequency stability of this signal is limited only by the stability of the primary oscillator, and the carrier is at least 60 db above noise power/cps. This phase-stabilization scheme will allow large averaging times, and hence step up intensity and precision of beam spectroscopic measurements.

3. Measurements with Ammonia

Figure 17 shows the 3-3 transition of ammonia, as measured with our system. The linewidth is measured by two frequency markers that are spaced 8 kc apart. A half-half-linewidth of 3 kc was obtained. The signal-to-noise ratio was 3. The line was observed in emission and in absorption. The absorption line showed an intensity that was 10 per cent of the predicted intensity; the emission lines showed only 1 per cent of the predicted intensity. (These experiments were performed with a traveling-wave structure instead
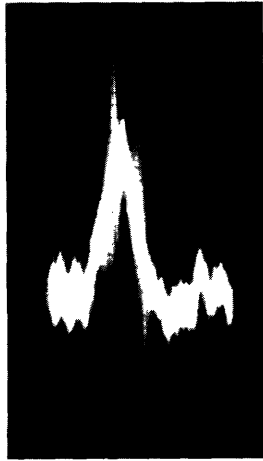
41

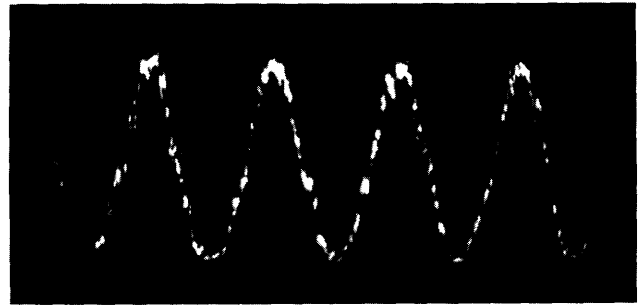Fig. 17. Emission spectrum of the ammonia 3-3 line.

Fig. 18. 500-cps beat between two phase-stabilized K-band klystrons.

of the resonant cavity.) The low state-selection efficiency can be explained by the fact that our selector rods were not liquid-nitrogen-cooled and that scattering reduced the efficiency. For sodium chloride, the selector should not show this defect.

IV. FREQUENCY DEFINITION

4.1 EFFICIENCY OF FREQUENCY MEASUREMENTS

Brillouin (37) has shown that if S indicates the entropy increase connected with a measurement, and I indicates the information gained by it, the following inequality holds

$$\frac{\Delta I}{\Delta S} = \mathscr{E} \leqslant 1 \tag{42}$$

Therefore $\mathscr{E}$ is a measure of the efficiency of an experiment in which an amount of entropy is traded for information. It turns out that for measurements such as frequency determinations, we have

$$\Delta I = k \ln A \tag{43}$$

Here, A, the accuracy of the experiment, is given by the interval in which we suspect the value to be, divided by the error left after the measurement has been performed. The reliability R is inversely proportional to the probability P_f that our measurement was in error, since a spurious thermal-noise signal was taken for the signal. In a more accurate treatment R would appear in Eq. 43. This is the case, for example, in the treatment of radar measurements by Woodward (38). His exact treatment bears out the fact that down to rather low R (R≈2), Eq. 43 is essentially correct.

We shall now indicate how to carry out a high-efficiency frequency measurement. We build a lossless interaction space and place molecules in it which are ready to absorb the radiation of a frequency, $\omega_o \mp 1/2\Delta\omega$. All we know a priori is that $\omega_a < \omega_o < \omega_b$. We divide the interval (ω_a, ω_b) into n cells of width $\Delta\omega$ and carry out the measurement by sending a certain amount of radiation into the interaction space at each different frequency. The radiation will then be reflected back; therefore no energy has been used except at the resonant frequency, at which frequency the energy will be absorbed. Brillouin shows that the amount of energy that will be spent for a measurement of accuracy A = n and reliability R is $\Delta E = (kT) \ln (nR)$. Thus we find that our spectroscope operates with efficiency

$$\mathscr{E} = \frac{\ln A}{\ln(nR)} = 1 \left/ \left(1 + \frac{\ln R}{\ln n} \right) \right. \tag{44}$$

In its present form, this measurement would be hard to realize. Recovery of the energy, for example, would be difficult. We might imagine, let us say, that the power bounces back from the interaction space and is re-reflected from a moving wall, and thus has a Doppler-shift frequency. But it is more practical to analyze an existing apparatus, such as the maser oscillator (11). During the minimum response time of the maser, $\tau \approx 10^{-4}$ sec, we obtain a relative error $\langle\Delta\omega^2 A\rangle^{1/2}/\omega = 10^{-10}$. If we divide the cavity

43

Q by this number (the cavity passband represents our a priori interval (ω_b, ω_a), we obtain $A = 10^6$. The amount of entropy produced is given by $\Delta S = (P_o \times \tau)/T = 300$ k, with $P_o = n\, h\nu = 1.4 \times 10^{-13}$ watt. Thus we obtain an efficiency $\mathscr{E} = 0.05$. This experiment is, therefore, very efficient. Why is it, then, not of optimum efficiency? Note that the wave train of 10^{-4}-sec duration has a "natural spectral width" $\Delta\omega_n \approx 2/\tau = 2 \times 10^4$ cps.

The accuracy achieved corresponds to a measurement with an error that is 1600 times smaller than the natural spectral width. This is possible (39) because in this experiment the voltage signal-to-noise ratio, r, is greater than 1600. However, the increase in accuracy has to paid for by a loss in efficiency. It is often possible to decrease the statistical error of any measurement by repeating the measurement many times and taking the average result. (Systematic errors, however, will not be decreased.) But a lot of redundant information is obtained, and therefore it is more efficient to design the experiment from the outset so that it will give the result with the desired accuracy.

In order to obtain nearly optimum performance, we must design a spectroscope with a sufficiently narrow natural spectral width, and a long time is required for making the experiment. This time requirement restricts the ultimate achievable precision in the same way that the energy requirement limits the accuracy of a time measurement (37). Both requirements are connected with the uncertainty principle. The efficiency considerations given here are among the reasons for building high-resolution spectrometers such as the molecular-beam microwave spectroscope. (Other reasons are the achievement of low systematic error, cavity pulling, and the physical interest in high resolution.)

Equation 44 illustrates the fact that an optimum design calls for a sacrifice in reliability. In an experiment with optimum design, the phenomenon to be observed is not too well distinguished from the noise background. Thus it often happens that great difficulties are encountered in realizing an experiment designed for optimum precision.

4.2 FREQUENCY PULLING

We have mentioned that if a spectral line of width $\Delta\nu_L$ is measured in a cavity of width $\Delta\nu_c$, and the cavity is detuned from the line resonant frequency ν_L by an amount $\delta\nu$, then Eq. 38 gives us the difference $d\nu$, between ν_L and the frequency of the maximum of the observed signal, ν_m.

Recently, Hermann and Bonanomi (40) have shown that injection of a proper signal will balance out the mode of a cavity. That this is so can also be seen from the form of the reflection coefficient of a cavity filled with radiating gas. We have

$$\Gamma = 2\delta_A \Big/ \left[\delta_o + \delta_A + \mathscr{E}_2 + 2i\left(\mathscr{E}^{1/2}\nu - \nu_c\right)\Big/\nu_L \right] - 1 \qquad (45)$$

where $1/\delta_A$ is the external Q, $1/\delta_o$ is the unloaded Q, and $\mathscr{E} = \mathscr{E}_2 + i\,\mathscr{E}_1$ is the

dielectric constant. For $\mathscr{E} = 0$, Γ is related to $i\nu$ by bilinear conformal mapping, hence the ν-axis is mapped into a circle. Injection of a proper constant signal will translate the origin of the circle to $\Gamma = 0$, and hence the cavity mode will not appear in an amplitude-sensitive detector. Hermann and Bonanomi also give the signal from the balanced cavity for $\mathscr{E} = 0$.

$$\Gamma^2 = \frac{\delta_1^2}{(\delta_1 + \delta_0)^2} - \frac{\mathscr{E}_2}{\left[(\delta_0 + \delta_1 + \mathscr{E}_2)/2\delta_1\right]^2 + \left[\mathscr{E}_1^{1/2}(\nu - \nu_L)/\delta_1 \nu_L\right]^2} \tag{46}$$

It has been stated elsewhere (11) that, in this case, the frequency pulling is given by Eq. 46.

How far does cavity pulling limit the accuracy of frequency measurements? It has been shown by Gordon, Zeiger, and Townes (11) that resonant absorption in a cavity gives essentially the cavity mode, with the distorted line resonance superposed. By tuning the cavity so that the line resonance lies first on the left and then on the right half-power point of the cavity resonance, we can determine the resonant frequency of the cavity. If the cavity has a normalized gain characteristic

$$G(\nu) = \frac{\Delta\nu_c}{\Delta\nu_c^2 + (\nu - \nu_c)^2}$$

it has a slope $1/(2\Delta\nu_c)$ at half-power points, and hence, since

$$G(\nu) + \frac{d}{d\nu} G(\nu)\, \delta\nu = G(\nu)(1 + \frac{2}{r})$$

where r is the signal-to-noise ratio, we obtain

$$\delta\nu = \frac{\Delta\nu_c}{r}$$

This gives us

$$d\nu = \frac{\Delta\nu_L}{r}$$

Thus we find that it is possible to adjust the cavity so that the pulling is no greater than the statistical readout error.

A severe limitation of this theory is that Eq. 38 is only approximately valid. Asymmetry in the cavity mode will introduce systematic errors.

CONCLUSION

We are interested in the quantum-mechanical behavior of molecular beams that inter-act with electromagnetic radiation. This interest includes an understanding of the energy spectrum in its finest details. This spectrum may be known either from previous meas-urements, from extrapolation from other measurements, or from order-of-magnitude calculations that will be confirmed in the operation of the beam device. We feel that the fine details of the spectra of most molecules of interest can be handled theoretically in a preliminary way, given sufficient time and interest to carry out the calculations that past experience has shown we can handle with a large amount of truth.

One extension of these calculations that is necessary for treating the general mole-cule is the calculation of high-field Stark effect. The amount of effort that must be spent upon further calculations depends, of course, upon the actual molecule used. The rotational-inversion energy spectrum of the ammonia molecule, for example, is such that we can neglect the high-field effects and still maintain a credible picture for the behavior of the molecule in the state selector. The use of symmetric tops and, in par-ticular, the asymmetric rotor, will require further computations of the Stark effect. We have confidence that the methods applied to the linear rotor will allow some simplifica-tion of these Stark-effect calculations, but we have not proceeded far enough to demon-strate a practical solution. Of course, the difficulties inherent in symmetric — and asymmetric — rotor calculations can be circumvented by choosing a molecule — ammonia, for example — that happens to have a simplified Stark effect for the energy levels that are of interest. Such a procedure does not aid in generalizing beam devices, since we gain our understanding of a particular physical phenomenon only from an analytical accident.

The general problem of the acceptance angle of a selector is not a property of the selector itself, given in terms of the available potentials and breakdown characteristic, but is truly defined by the slopes of the energy levels in the presence of an electric field. This means that generalized rational design of beam devices requires more than simple scaling factors for evaluating the beam flux from the effective acceptance angle. The field of state-selector design seems to be trapped in the fascination of an initial maxi-mum, in that the multipole state selectors of Bennewitz, Paul, and Schlier (16) have operated so successfully for ammonia that there is little incentive to try other state-selecting configurations. We feel that there is a good deal of rewarding work that could be done in the field of generalizing state-selector designs. It is apparent that great effort must be expended in order to analyze any single selector design properly. Thus from the point of view of scientific return this field is probably an inefficient one in which to work. In spite of this fact, laboratory experiments, which are now in the design stage, will be carried out.

The method of observing the absorption or emission of electromagnetic energy from a molecular beam formed in the apparatus can be analyzed by means of a fairly well-understood theory. The problem is mainly one of matching from the beam into the

electromagnetic field. A resonant matching device is conventionally used. Although it was not apparent when we started to work in this field, it is now certainly indicated that mode control can be realized by our techniques. Any analysis of the efficacy of beam frequency standards will indicate that as strong a beam as possible should be established. Our effort to understand the natural limitations on beam flux has indicated that the most readily attainable limitation is that imposed by beam self-thermalization. By this we mean that thermalizing interactions within some degrees of freedom of a molecular beam are more rapid than they are within others. In fact, it can be shown that the translational degree of freedom, which defines the spatial structure of the molecular beam, is much less sensitive to molecular density than are the rotational-vibrational degrees of freedom. This means that the interactions that can occur in a dense beam tend to establish thermal equilibrium within the actual beam operational levels at beam densities that are now available in the laboratory. Thus we are in a position to predict maximum power-operating levels for molecular-beam devices. This subject can be considered as understood from theory and by extrapolation from other data, but it is not understood experimentally from observations on operating maser devices.

The difference in the available signal power from either an active or a passive beam device — that is, one operated either as a regenerative oscillator or as a straight absorption or emission spectrograph — is quite trivial. Practical factors will dictate whether active or passive operation is optimum for the realization of a time or frequency standard. It is not at all obvious that we have sufficient understanding of the problem to define an optimum time or frequency standard. There is a fascinating simplicity in an oscillating device, in that it supplies its own electromagnetic signal for defining a frequency. What frequency is actually defined by this electromagnetic radiation is not at all obvious. In other words, we are looking only at the _effect_. It has previously been contended that knowledge of, and control over, the stimulating or activating electromagnetic radiation and observation of the effect of the frequency-determining system on the electromagnetic radiation will yield more useful information for defining a standard frequency. The additional information that has been made available from measuring the complex interaction function of the total observation system allows corrections for extraneous observational effects, such as the shift in cavity resonance frequency, and other dispersions in the observational system (41).

It is not entirely clear how the application of the concept of efficiency in time- and frequency-measuring processes is to be applied to the problem of realizing an optimum time or frequency standard. In any case, the concept of the efficiency of frequency measurements is a physical parameter of an observational system. The efficiency concept can be used as a strong argument for high-resolution, low-sensitivity frequency standards. Stated otherwise, it can be shown that the precision of a frequency definition depends not only upon the intrinsic resolution of the apparatus, but also upon the signal-to-noise ratio. We are therefore confronted with the question, Should we use a low-resolution, high signal-to-noise apparatus or should we use a high-resolution, low

signal-to-noise apparatus, or is a compromise system possible? If we apply the concept of efficiency to the problem, we are led to the conclusion that it is best to build a high-resolution apparatus with the concomitant low signal-to-noise ratio in order to achieve both high precision and high efficiency. Low-resolution, high signal-to-noise-ratio devices suffer from the fact that, as is known from information theory, information increases at a very low rate once ambiguities have been resolved. In other words, once the presence of an absorption signal is indicated, a great deal of signal energy must be expended in order to define the center of the resonance as precisely as a small fraction of the total width. The problem is elusive and we have not solved it to the point of obtaining a logical design for optimum frequency-defining apparatus.

The signal-to-noise ratio is given by

$$r = \sqrt{n} \sqrt{\frac{h\nu}{kT}}$$

There are ways of making the second factor equal to unity. In the molecular-beam method, in which the n molecules are counted, there is no need to match the radiation by means of a high-Q cavity, and thereby pulling is diminished. Another means of efficient counting is the use of the double-resonance method (42). The use of quantum-mechanical amplifiers also permits working at sufficiently low noise temperatures, in order to make the second factor equal to unity (25).

Finally, a beam device might be operated at sufficiently high frequency and reach the same goal. The method of beam spectroscopy seems, therefore, to give promise for making spectroscopic precision measurements. For each element of the procedure — selection, excitation, and detection of resonances — several methods are available, and the best one must be chosen.

References

1. M. W. P. Strandberg and H. Dreicer, Phys. Rev. $\underline{94}$, 1393 (1954).

2. J. P. Gordon, J. J. Zeiger, and C. H. Townes, Phys. Rev. $\underline{95}$, 982 (1954).

3. H. E. D. Scovil, G. Feher, and H. Seidel, Phys. Rev. $\underline{105}$, 762 (1957).

4. M. W. P. Strandberg, Microwave Spectroscopy (Methuen and Co., Ltd., London, 1954).

5. H. R. Johnson and M. W. P. Strandberg, J. Chem. Phys. $\underline{20}$, 687 (1952).

6. M. Tinkham, Theory of the fine structure of the molecular oxygen ground state with an experimental study of its microwave paramagnetic spectrum, Ph.D. Thesis, Department of Physics, M.I.T., June 1954; Phys. Rev. $\underline{97}$, 937 (1955).

7. C. H. Townes and A. L. Schawlow, Microwave Spectroscopy (McGraw-Hill Publishing Company, New York, 1955); see especially Chapter 8.

8. A. Simon, J. H. Vander Sluis, and L. C. Biedenharn, Report 1679, Oak Ridge National Laboratory, 1954.

9. R. A. Frosch and H. M. Foley, Phys. Rev. $\underline{88}$, 1337 (1952).

10. E. U. Condon and G. H. S. Shortley, The Theory of Atomic Spectra (Cambridge University Press, London, 1951), p. 70.

11. J. P. Gordon, H. J. Zeiger, and C. H. Townes, Phys. Rev. $\underline{99}$, 1264 (1955).

12. R. A. Logan, R. E. Coté, and P. Kusch, Phys. Rev. $\underline{86}$, 280 (1952).

13. B. P. Dailey and C. H. Townes, J. Chem. Phys. $\underline{23}$, 118 (1955).

14. C. A. Lee, B. P. Fabricand, R. O. Carlson, and I. I. Rabi, Phys. Rev. $\underline{91}$, 1395, (1953).

15. A. Honig, C. H. Townes, M. L. Stitch, and M. Mandel, Phys. Rev. $\underline{96}$, 634 (1954).

16. H. G. Bennewitz, W. Paul, and C. Schlier, Z. Physik $\underline{141}$, 6-15 (1955).

17. H. K. Hughes, Phys. Rev. $\underline{72}$, 614 (1947).

18. C. Schlier, Z. Physik $\underline{141}$, 16 (1955).

19. J. Barriol, J. phys. radium $\underline{11}$, 62 (1950).

20. L. Pauling and B. Wilson, Introduction to Quantum Mechanics (McGraw-Hill Book Company, Inc., New York, 1935).

21. W. H. Schaffer, Revs. Modern Phys. $\underline{16}$, 245 (1944).

22. R. H. Dicke, Phys. Rev. $\underline{93}$, 99 (1955).

23. R. H. Dicke and R. H. Romer, Rev. Sci. Instr. $\underline{26}$, 915 (1955).

24. W. Heitler, Quantum Theory of Radiation (Oxford University Press, London, 2d ed., 1944).

25. M. W. P. Strandberg, Phys. Rev. $\underline{106}$, 617 (1957); Errata, Phys. Rev. $\underline{108}$, 1648 (1957).

26. T. C. Wang, Bull. Am. Phys. Soc., Ser. 2, Vol. 2, p. 209 (April 25, 1956).

27. K. Shimoda, T. C. Wang, and C. H. Townes, Phys. Rev. $\underline{102}$, 1308 (1956).

28. H. R. Johnson and M. W. P. Strandberg, Phys. Rev. $\underline{86}$, 811 (1952).

29. C. H. Townes and S. Geschwind, J. Appl. Phys. $\underline{19}$, 795 (1948).

30. S. Datz and E. H. Taylor, J. Chem. Phys. $\underline{25}$, 389 (1956).

31. R. C. Miller and P. Kusch, Phys. Rev. $\underline{99}$, 1314 (1955).

32. S. Silver, Microwave Antenna Theory and Design, Radiation Laboratory Series Vol. 12 (McGraw-Hill Book Company, Inc., New York, 1949).

33. R. H. Rearwin, Microwave frequency standard, S.M. Thesis, Department of Electrical Engineering, M.I.T., May 1954.

34. R. V. Pound, Microwave Mixers, Radiation Laboratory Series Vol. 16 (McGraw-Hill Book Company, Inc., New York, 1948).

35. M. Peter and M. W. P. Strandberg, Proc. IRE 43, 869 (1955).

36. N. Sawazaki and T. Honma, A new frequency standard by quenching oscillator control, Trans. IRE, vol. MTT-4, no. 2, p. 116 (April 1956).

37. L. Brillouin, Science and Information Theory (Academic Press, Inc., New York, 1956).

38. P. M. Woodward, Probability and Information Theory (McGraw-Hill Book Publishing Company, Inc., New York, 1953).

39. M. W. P. Strandberg, H. R. Johnson, and J. R. Eshbach, Rev. Sci. Instr. 25, 776 (1954).

40. J. Hermann and J. Bonanomi, Helv. Phys. Acta 29, 448 (1956).

41. M. W. P. Strandberg, paper presented at the Symposium on Generation, Stabilization, and Amplification of Electromagnetic Oscillations by Atomic and Molecular Resonances, Asbury Park, New Jersey, February 1956.

42. H. G. Dehmelt, Phys. Rev. 105, 1924 (1957).